

**On the theory of Biot-patchy-squirt mechanism for wave propagation in
partially saturated double-porosity medium**

Weitao Sun^{1,2}

¹School of Aerospace Engineering, Tsinghua University, Beijing, 100084, China

²Zhou Pei-Yuan Center for Applied Mathematics, Tsinghua University, Beijing,
100084, China

Corresponding author: Weitao Sun, sunwt@tsinghua.edu.cn

¹ Weitao Sun, School of Aerospace Engineering, Tsinghua University, Beijing, 100084, China,
sunwt@tsinghua.edu.cn

Abstract

Reservoir rocks are usually composed of a coherent heterogeneous porous matrix saturated by multiple fluids. At long wavelength limit, the composite material of solid skeleton is usually regarded as homogeneous media. However, at grain scale or high loading rate, non-uniform fluid flow at internal interface of heterogeneity plays essential role in wave dispersion and attenuation. Formulating wave propagation in partially saturated and fractured rocks is challenging and of great interests in geoscience. Here we raise a Biot-patchy-squirt (BIPS) model to characterize wave dispersion/attenuation in fractured poroelastic media saturated by two immiscible fluids. BIPS model incorporates the mechanism of local fluid-interface flow (LFIF) and squirt flow into global fluid flow simultaneously. Theoretical analysis show that wave attenuations caused by viscous dissipation, squirt flow and patchy interface vibration are distinct from each other. BIPS is intrinsically consistent with Biot theory, squirt and LFIF model and reduces to such mechanism in limiting conditions. More interestingly, numerical results show that coupling between LFIF and squirt flow is of evident importance to P-wave dispersion and attenuation. Comparisons with experimental data indicate that BIPS model is computationally reliable and in reasonably good agreement with experimental data. This study advance our understanding of the fundamental physics of wave propagation in natural reservoir rocks and push forward the potential applications of the triple dispersion/attenuation mechanism to wave velocity estimation in deep earth.

Keywords: wave dispersion/attenuation, Biot's theory, patch saturation, squirt flow

Introduction

In the last decades, wave dispersion and attenuation in natural reservoir rocks attract more and more attentions (Dutta and Ode, 1979, Norris, 1993, Dvorkin *et al.*, 1995, Sams *et al.*, 1997, Berryman and Wang, 2000, Johnson, 2001, Pride *et al.*, 2004, Berryman and Pride, 2005, Carcione and Picotti, 2006, Toms *et al.*, 2006, Toms *et al.*, 2007, Rubino and Holliger, 2012, Ba *et al.*, 2015, Sun *et al.*, 2016, Sharma, 2017, Zheng *et al.*, 2017). Intrinsic attenuation is believed mainly come from fluid flow in saturated rocks, which is driven by pressure gradient through 'Darcy's law'. Although the theory of wave propagations in single porosity and fully saturated porous medium have been well established since Biot (Biot, 1956, Biot, 1962), energy dissipation mechanisms in tight rock with low porosity/permeability remain poorly understood. Experimental observations question the universal validity of single

dispersion/attenuation mechanism caused by fluid-solid viscous dissipation in single porosity postulation (Winkler, 1985, Winkler, 1986).

Natural reservoir rocks are usually heterogeneous porous medium made up of mineral grains and cements materials. P wave dispersion and attenuation arise when scattering occurs at inhomogeneity interface, fluid/solid interaction and squirt flow in fractures/cracks. Pore/cracks structure are important source of matrix heterogeneity. Barenblatt *et al.* (Barenblatt *et al.*, 1960) studied double-porosity continuum model with fluid exchange between matrix pore and fracture. Multi-porosity models were proposed based on mass-momentum-energy balance equations by Aifantis (Aifantis, 1977, Aifantis, 1980, Aifantis, 1979), Wilson and Aifantis (Wilson and Aifantis, 1982), Khaled *et al.* (Khaled *et al.*, 1984), Elsworth and Bai (Elsworth and Bai, 1992). Bai *et al.* (Bai *et al.*, 1993, Bai, 1999) studied the deformation-dependent flow models. Berryman and Wang (Berryman and Wang, 1995, Berryman and Wang, 2000) formulated wave propagations in double-porosity medium. Chapman incorporated meso-scale anisotropic fracturing into the grain scale fluid flow model (Chapman *et al.*, 2002).

In addition to solid skeleton heterogeneity, immiscible fluid patches are another important source of attenuation. In oil recovery, time-lapse seismic monitoring and CO₂ injection, the acoustic properties of rock saturated by two immiscible fluids are of great interests. Many efforts have been made to set up the quantitative relationships between wave velocities and fluid saturation (White, 1975, White *et al.*, 1975, Dutta and Ode, 1979, Dutta and Odé, 1979, Dutta and Seriff, 1979, Johnson, 2001, Pride *et al.*, 2004, Ba *et al.*, 2011, Sun *et al.*, 2016, Müller and Gurevich, 2004, Müller *et al.*, 2008). Experimental observations have been reported about the velocity-saturation relation in sonic and ultrasonic frequency bands (Gregory, 1976, Wyllie *et al.*, 1958, Wyllie *et al.*, 1956, Murphy, 1984, Cadoret *et al.*, 1995, Cadoret *et al.*, 1998, Bacri and Salin, 1986). Wave-induced fluid flow due to mesoscopic heterogeneity is believed as the one of the main mechanism underlining the energy dissipation in partially saturated rocks (Toms *et al.*, 2006, Müller and Gurevich, 2004, Berryman and Pride, 2005, Johnson, 2001). What's more, fluid patch size and spatial distribution are important factors controlling wave dispersion and attenuation (Helle *et al.*, 2003, Toms *et al.*, 2006, Sun *et al.*, 2015, Lebedev *et al.*, 2009, Lopes and Lebedev, 2012). The effects of randomly distributed fluid patches have also been studied by Toms *et al.* (Toms *et al.*, 2007). The coexistence of solid-fluid heterogeneity has been studied by a triple-layer patchy (TLP) model (Sun *et al.*, 2016). Experimental results indicate injection rate may control the patch formation (Toms-Stewart *et al.*, 2009, Lopes *et al.*, 2014, Liu *et al.*, 2016).

Consider a saturated rock with fractures and cracks, the fissured part has greater deformations than the inter-granular pores and result in a squirt flow from cracks to pores. It is believed that attenuation can be dominated by the squirt flow between pores of different shapes and orientations at sonic and ultrasonic frequencies (Mavko and Nur, 1975). Microscopic “squirt flow” mechanism has been developed to explain the measured attenuation and velocity dispersion (Oconnell and Budiansky, 1977, Thas, 2007, Mavko and Nur, 1979, Dvorkin *et al.*, 1995, Dvorkin and Nur, 1993, Gurevich *et al.*, 2010, Chapman *et al.*, 2002). Evidence of squirt flow in sandstone has been reported based on the laboratory observation of seismic attenuation (Subramaniyan *et al.*, 2015b). Comparisons between experimental data and simulation results imply that at ultrasonic frequencies the squirt flow is due to the presence of clay (Marketos and Best, 2010).

On one hand, Biot-squirt (BISQ) model in single-porosity rocks (Dvorkin and Nur, 1993, Dvorkin *et al.*, 1995) is based on Biot’s theory and squirt flow mechanism. On the other hand, wave propagation in partially saturated double-porosity matrix with heterogeneous patches is formulated based on both Biot theory and local fluid-interface flow (LFIF) mechanisms (Sun *et al.*, 2016, Johnson, 2001, Pride *et al.*, 2004, Rubino and Holliger, 2012, Berryman and Wang, 2000). However, to our knowledge, detailed work on the relationship among global fluid flow, LFIF and squirt flow is still missing. Despite the importance from both the theoretical and applied points of view, the laws governing immiscible two-phase flow through heterogeneous double-porosity (pore-fracture) materials is still uncovered.

It is recognized that Biot global flow, squirt flow and LFIF are distinct from each other. The patchy-saturation effect can be weakened by squirt flow effect in sandstones (Johnson, 2001). Relative importance of global and squirt flow has also been investigated (Ali and Jakobsen, 2014). Recently, the velocity-saturation relations obtained for various injection rates show that patch size may increase with fluid saturation and decrease with injection rate (Liu *et al.*, 2016). Since squirt flow is closely related to injection rate, the results imply that patch saturation and squirt flow may have uncovered relation with each other. Unfortunately, how the dispersion/attenuation depend on the interactions of global flow, LFIF and ‘squirt flow’ remains poorly understood.

The work of combining Biot theory, patchy saturation model and squirt flow model was first used to study rocks in partially saturated complex pore reservoirs (Sun, 2018). The main goal of this study is to formulate Biot-patchy-squirt (BIPS) flow for wave propagations in partially saturated double-porosity media. Here the three important energy dissipation sources, say Biot theory, patchy saturation and squirt flow model, are believed to be intrinsically

interconnected at multiple spatial scale and full range of time scale. Therefore, we aim to establish a consistent formulation connecting Biot, patchy saturation and squirt flow mechanisms in a well-defined way.

The formulation in this work has two main parts. (1) The wave equations of Biot-patchy-squirt mechanism is formulated based Lagrangian equations, mass conservation equations and constitutive equation of double-porosity media. (2) The consistence among BIPS, Biot, BISQ and patchy models is analysed in limiting conditions. In the examples section, we numerically predicted P wave velocity for oil-brine saturated French Vosgian sandstone. Comparison with experimental data demonstrate that BIPS model successfully catch the multiple frequency dispersions and the predicted velocities are in reasonably good agreement with laboratory observations.

Method

Dynamic equations of Biot-patchy model

Biot-patchy model incorporates solid-fluid heterogeneities by introducing patches embedded in a homogeneous host medium. In a cubic representative element volume (REV), the solid matrix is partitioned into inclusion and host parts by interface S_{solid} (Figure 1 (a)). The heterogeneous matrix have double-porosity, i.e., the inner spheroid inclusion region with porosity ϕ_{in} and the surrounding host region with porosity ϕ_{host} . The radii of inclusions are much smaller than the P-wavelength but much larger than the pore size (mesoscopic scale). The interface S_{solid} between inclusions and host medium is open and fluids can flow through it. The host region is represented as an equivalent concentric shell (Figure 1 (a)).

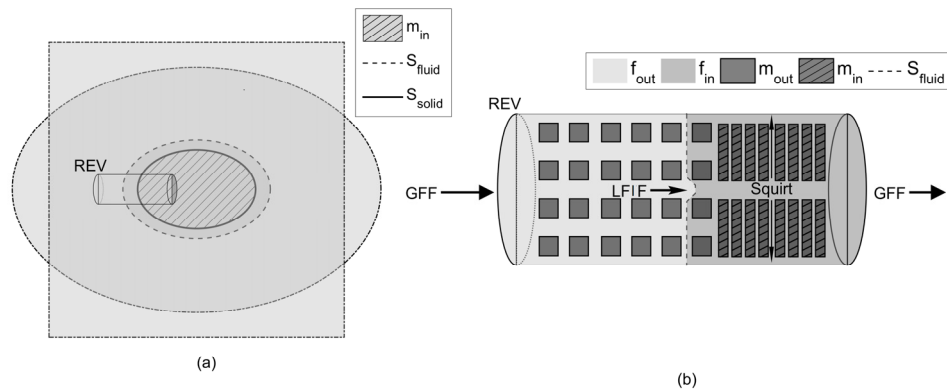


Figure 1 Schematic diagram of Biot-patchy-squirt model. (a) Porous matrix with heterogeneities m_{in} (hatched patches) are partially saturated by immiscible fluid f_{out} (background) and f_{in} (dark shaded patches). The outside cubic patch volume is represented by an equivalent spheroid. S_{solid} is the solid heterogeneity

interface. S_{fluid} is the fluid heterogeneity interface. (b) A cylindrical representative element volume (REV) containing double porosities and two immiscible fluids. Global fluid flow (GFF) occurs at larger scale level. Local fluid-interface flow (LFIF) occurs at the patch interface. Squirt flow occurs in the solid heterogeneities m_{in} (hatched patches).

Two immiscible fluids saturate the double-porosity skeleton. An interface S_{fluid} exists between the inner fluid pocket and the outside fluid zone (Figure 1(a)). The fluid interface S_{fluid} does not necessarily overlap S_{solid} . In fact, the solid matrix and pore fluid patch are two independent heterogeneous systems and need to be treated separately. The inner fluid pocket may cover across S_{solid} . Nevertheless, the surrounding matrix saturated by the other fluid can also contain both porosities when S_{fluid} is inside S_{solid} . Based on such an ‘‘triple-layer patchy’’ (TLP) model, wave equations are obtained (Sun *et al.*, 2016).

The kinetic energy of the TLP system is:

$$T = \frac{1}{2} \sum_{i=1}^3 \rho_{00} \dot{u}_i^2 + \sum_{i=1}^3 \sum_{m=1}^2 \rho_{0m} \dot{u}_i \dot{U}_i^{(m)} + \frac{1}{2} \sum_{i=1}^3 \sum_{m=1}^2 \rho_{mm} \dot{U}_i^{(m)2} + \frac{\phi_1 \phi_2^2}{6} \dot{\zeta}^2 \chi_1, \quad (1)$$

where $U_i^{(m)}$ is the fluid displacements in the m -th fluid regions and $\chi_1 = a_{20}^2 v_1^{2/3} [\rho_{f_1} + \rho_{f_2} (\phi_{10}/\phi_{20}) \cdot (1 - a_{10}/a_{20})]$. Here $m=1$ denotes the inner fluid pocket and $m=2$ is the surrounding fluid patch. u_i is the mesoscopic volume average displacement of solid skeleton. The definitions of density coefficients are $\rho_{mm} = \rho_{f_m} \phi_m (1 + 1/\phi_{m0})/2$,

$\rho_{0m} = \rho_{f_m} \phi_m (1 - 1/\phi_{m0})/2$ and $\rho_{00} = \rho_0 - \sum_{m=1}^2 \rho_{f_m} \phi_m (1 - 1/\phi_{m0})/2$ (Sun *et al.*, 2016), where

$\rho_0 = \sum_{m=1}^2 v_m (1 - \phi_{m0}) \rho_{s_m}$ is the density of solid skeleton, ρ_{f_m} are the fluid densities in the m -th

type of fluid patch. $v_2 = 1 - v_1$ is the volume fraction of the surrounding fluid patch. a_{10} and a_{20} are the radii of concentric fluid patches.

The strain energy is

$$W = \frac{1}{2} [(A + 2N)I_1^2 - 4NI_2 + 2Q_1 I_1 (\xi_1 - \phi_2 \zeta) + R_1 (\xi_1 - \phi_2 \zeta)^2 + 2Q_2 I_1 (\xi_2 + \phi_1 \zeta) + R_2 (\xi_2 + \phi_1 \zeta)^2], \quad (2)$$

where I_1 and I_2 are the first and second strain invariants of solid matrix. ξ_m are the first strain invariants of the average fluid displacement $\mathbf{U}^{(m)}$ ($m = 1, 2$). N is the average shear modulus of the solid matrix. $A, Q_m, R_m, (m = 1, 2)$ are stiffness coefficients calculated from the porosity ϕ , the frame bulk modulus K_b , and the solid and fluid bulk moduli K_s, K_f .

The dissipation function of TLP model is

$$D = \frac{1}{2} \sum_{m=1}^2 b_m \sum_{i=1}^3 (\dot{U}_i^{(m)} - \dot{u}_i)^2 + \frac{\phi_1 \phi_2^2}{6} \zeta^2 \beta_1, \quad (3)$$

where $b_m = v_m \phi_{m0}^2 \eta_m / \kappa_m$ ($m=1,2$) is the viscous resistance coefficients and κ_m is the permeability. η_m, v_m are the viscosity and volume fractions. Here we introduced following notations $\kappa_1 = \langle \kappa \rangle_{in}$ and $\kappa_2 = \langle \kappa \rangle_{host}$. The term related to LFIF is $\beta_1 = v_1^{2/3} \phi_{10} a_{20}^2 [b_1 + b_2 (1 - a_{10}/a_{20})]$.

Regarding the Euler-Lagrange equations with dissipation function, the dynamic equations are:

$$\rho_{00} \ddot{\mathbf{u}} + \sum_{m=1}^2 [\rho_{0m} \ddot{\mathbf{U}}^{(m)} + b_m (\dot{\mathbf{u}} - \dot{\mathbf{U}}^{(m)})] = \nabla \cdot \boldsymbol{\sigma},$$

$$\rho_{01} \ddot{\mathbf{u}} + \rho_{11} \ddot{\mathbf{U}}^{(1)} + b_1 (\dot{\mathbf{U}}^{(1)} - \dot{\mathbf{u}}) = \nabla s_1,$$

$$\rho_{02} \ddot{\mathbf{u}} + \rho_{22} \ddot{\mathbf{U}}^{(2)} + b_2 (\dot{\mathbf{U}}^{(2)} - \dot{\mathbf{u}}) = \nabla s_2, \quad (4)$$

$$-(\chi_1 \ddot{\zeta}_1 + \beta_1 \dot{\zeta}_1) \frac{\phi_1 \phi_2^2}{3} = \phi_2 s_1 - \phi_1 s_2,$$

where $\boldsymbol{\sigma} = \frac{\partial W}{\partial \mathbf{e}}$, $s_1 = \frac{\partial W}{\partial \xi_1}$, $s_2 = \frac{\partial W}{\partial \xi_2}$. Here \mathbf{e} is the strain tensor of solid frame. $\zeta = \nabla \cdot \mathbf{Z}$

is the increment of local fluid flow caused by the pressure difference between different fluid patches. \mathbf{Z} is the local fluid flow between immiscible fluid patches. The viscous resistance coefficients can also be written as $b_m = \rho_{f_m} \phi_m \omega_c^{(m)}$ ($m=1,2$). Here $\omega_c^{(m)} = \frac{\mu_m \phi_{m0}}{\rho_{f_m} \kappa_m}$ are the characteristic frequency for immiscible fluid patches. The scalar s_1, s_2 are related to fluid pressure by $s_1 = -\phi p_1$ and $s_2 = -\phi p_2$. p_1 and p_2 are the pressure in inner fluid pocket and outside fluid patch.

Wave equations of Biot-patchy-squirt (BIPS) model

Consider a cubic REV in the partially saturated double-porosity medium, which has a size larger enough than pores and patches but smaller enough than the macroscopic phenomena scale (such as the wave length). BISQ model provides a scenario of transverse fluid flow in a representative cylinder with its axis parallel to the direction of wave propagation. For single-porosity case, 2D mass conservation equations in x and r directions have been

given by Dvorkin and Nur (Dvorkin and Nur, 1993). Here we extend squirt flow mechanism to patch saturation in rocks with double porosity.

For the case of uniaxial deformation, we have axial dynamic equations

$$\begin{aligned}
\rho_{00}\ddot{u}_x + \rho_{01}\ddot{U}_x^{(1)} + \rho_{02}\ddot{U}_x^{(2)} + b_1(\dot{u}_x - \dot{U}_x^{(1)}) + b_2(\dot{u}_x - \dot{U}_x^{(2)}) &= \bar{M} \frac{d^2 u_x}{dx^2} - \gamma_1 \frac{dp_1}{dx} - \gamma_2 \frac{dp_2}{dx} \\
\rho_{01}\ddot{u}_x + \rho_{11}\ddot{U}_x^{(1)} + b_1(\dot{U}_x^{(1)} - \dot{u}_x) &= -\phi_1 \frac{\partial p_1}{\partial x} \\
\rho_{02}\ddot{u}_x + \rho_{22}\ddot{U}_x^{(2)} + b_2(\dot{U}_x^{(2)} - \dot{u}_x) &= -\phi_2 \frac{\partial p_2}{\partial x} \\
-(\chi_1 \zeta_x + \beta_1 \dot{\zeta}_x) \frac{\phi_1 \phi_2^2}{3} &= \phi_1 \phi_2 (p_2 - p_1)
\end{aligned} \tag{5}$$

where $\zeta_x = \frac{dZ_x}{dx}$ and Z_x is the local fluid flow between different fluid patches.

$$\bar{M} = \frac{M_1 M_2}{\nu_1 M_2 + \nu_2 M_1}, M_m = 2G_m \frac{1 - \nu_m}{1 - 2\nu_m}, m=1,2. \text{ Here } G_m \text{ and } \nu_m \text{ are shear modulus and}$$

Poisson's ratio.

The radial dynamic equations are:

$$\begin{aligned}
\frac{\rho_{f_1}}{2} \phi_1 \left(1 + \frac{1}{\phi_{10}} \right) \ddot{U}_r^{(1)} + b_1 \dot{U}_r^{(1)} &= -\phi_1 \frac{\partial p_1}{\partial r} \\
\frac{\rho_{f_2}}{2} \phi_2 \left(1 + \frac{1}{\phi_{20}} \right) \ddot{U}_r^{(2)} + b_2 \dot{U}_r^{(2)} &= -\phi_2 \frac{\partial p_2}{\partial r}
\end{aligned} \tag{6}$$

The conservation equations in partially saturated double-porosity medium are given as (Appendix A)

$$\begin{aligned}
\frac{\phi_1}{\rho_{f_1}} \frac{\partial \rho_{f_1}}{\partial t} + \frac{\partial \phi_1}{\partial t} + \phi_1 \frac{\partial^2 (U_x^{(1)} - \phi_2 Z_x - u_x)}{\partial t \partial x} + \phi_1 \left(\frac{\partial^2 (U_r^{(1)})}{\partial t \partial r} + \frac{1}{r} \frac{\partial (U_r^{(1)})}{\partial t} \right) &= 0 \\
\frac{\phi_2}{\rho_{f_2}} \frac{\partial \rho_{f_2}}{\partial t} + \frac{\partial \phi_2}{\partial t} + \phi_2 \frac{\partial^2 (U_x^{(2)} + \phi_1 Z_x - u_x)}{\partial t \partial x} + \phi_2 \left(\frac{\partial^2 (U_r^{(2)})}{\partial t \partial r} + \frac{1}{r} \frac{\partial (U_r^{(2)})}{\partial t} \right) &= 0
\end{aligned} \tag{7}$$

Here $d\phi_m$ ($m=1,2$) is the porosity change, i.e., the variation in fluid content. In the case of plane-wave propagation, the displacements and pressure are expressed as $[u_x, U_x^{(1)}, U_x^{(2)}, U_r^{(1)}, U_r^{(2)}, Z_x, p_1, p_2] = [C_1, C_2^{(1)}, C_2^{(2)}, C_{r0}^{(1)}, C_{r0}^{(2)}, C_3, p_{01}, p_{02}] \cdot e^{i(\alpha t - \mathbf{k} \cdot \mathbf{x})}$.

Combing (5), (6), (7), we have the ordinary differential equations of p_{01} and p_{02} as

$$\begin{aligned} \frac{\partial^2 p_{01}}{\partial r^2} + \frac{1}{r} \frac{\partial p_{01}}{\partial r} + \frac{\rho_{f_1} \omega^2}{F_1} \left(\frac{1+1/\phi_{10}}{2} - i \frac{\omega_c^{(1)}}{\omega} \right) p_{01} - ik\rho_{f_1} \omega^2 \left(C_2^{(1)} - \phi_2 C_3 + \frac{\gamma_1}{\phi_1} C_1 \right) \left(\frac{1+1/\phi_{10}}{2} - i \frac{\omega_c^{(1)}}{\omega} \right) &= 0 \\ \frac{\partial^2 p_{02}}{\partial r^2} + \frac{1}{r} \frac{\partial p_{02}}{\partial r} + \frac{\rho_{f_2} \omega^2}{F_2} \left(\frac{1+1/\phi_{20}}{2} - i \frac{\omega_c^{(2)}}{\omega} \right) p_{02} - ik\rho_{f_2} \omega^2 \left(C_2^{(2)} + \phi_1 C_3 + \frac{\gamma_2}{\phi_2} C_1 \right) \left(\frac{1+1/\phi_{20}}{2} - i \frac{\omega_c^{(2)}}{\omega} \right) &= 0 \end{aligned} \quad (8)$$

This is the Bessel differential equation. Adopting pressure boundary condition

$p_{01} = p_{01}^*, p_{02} = p_{02}^*$ at pore wall $r = R$, we have pressures

$$\begin{aligned} p_{01} &= ikF_1 \left(C_2^{(1)} - \phi_2 C_3 + \frac{\gamma_1}{\phi_1} C_1 \right) \left(1 - \frac{J_0(\lambda_1 r)}{J_0(\lambda_1 R)} \right) + p_{01}^* \frac{J_0(\lambda_1 r)}{J_0(\lambda_1 R)} \\ p_{02} &= ikF_2 \left(C_2^{(2)} + \phi_1 C_3 + \frac{\gamma_2}{\phi_2} C_1 \right) \left(1 - \frac{J_0(\lambda_2 r)}{J_0(\lambda_2 R)} \right) + p_{02}^* \frac{J_0(\lambda_2 r)}{J_0(\lambda_2 R)} \end{aligned} \quad (9)$$

where $F_1 = \frac{K_{f_1}(\phi_1 + \phi_2 \beta) H_1}{K_{f_1} + (\phi_1 + \phi_2 \beta) H_1}$, $F_2 = \frac{K_{f_2}(\phi_2 + \phi_1 / \beta) H_2}{K_{f_2} + (\phi_2 + \phi_1 / \beta) H_2}$. J_0 is the zero order Bessel

function. p_{01}^* and p_{02}^* are pressure values at the boundary. The coefficient λ_1 , λ_2 are

$$\text{defined as } \lambda_1^2 = \frac{\rho_{f_1} \omega^2}{F_1} \left(\frac{1+1/\phi_{10}}{2} - i \frac{\omega_c^{(1)}}{\omega} \right) \text{ and } \lambda_2^2 = \frac{\rho_{f_2} \omega^2}{F_2} \left(\frac{1+1/\phi_{20}}{2} - i \frac{\omega_c^{(2)}}{\omega} \right).$$

Pressure in hard pore space

The squirt flow model has been developed for partially saturated rocks, in which the squirting flow is realized as cross-flow between fluid pore and gas pockets (Dvorkin and Nur, 1993). In such a case, the pressure boundary condition at pore wall $r = R$ is set to zero. At low frequency the velocity calculated by zero-pressure boundary condition drops to that of rock with gas rather than to Gassmann's values? This is related to the constant-pressure boundary conditions in the original BISQ(Dvorkin and Nur, 1993). However, when the rock is fully saturated by liquids, the zero-pressure boundary condition cannot provide accurate velocities. Squirt flow in fully saturated rocks has been formulated by Dvorkin, Mavko and Nur(Dvorkin *et al.*, 1995).

In this section, we will provide a solution of the boundary pressure for double porosity rocks. We consider a double porosity matrix made of linear elastic isotropic solid materials. The matrix is saturated by two liquids. The effective stress of the overall porous rock is (Appendix A)

$$\bar{\sigma}_x = \bar{M} \frac{du}{dx} - \alpha'_1 p_1 - \alpha'_2 p_2, \quad (10)$$

At low frequencies, the fluid pressure in compliant pore space will equilibrate, which lead to Gassmann's formula. At high frequencies, the fluids have no time to relax and become blocked, which can be regarded as a part of the matrix. If we introduce an effective matrix which has the same behavior as the original solid skeleton plus the soft pore filled with blocked fluids, the pressure in the left hard pores can be calculated as

$$\bar{\sigma}_x = M_{eff} \frac{du}{dX} - \alpha_{eff} p_1 - \alpha_{eff} p_2, \quad (11)$$

P-wave dispersion and attenuation

The dynamic equations of Biot-patchy-squirt model relate displacements U_x, u_x, Z_x to fluid pressure p . The pressure boundary condition plays an essential role in determining the bulk modulus and velocity of porous media. Zero pressure boundary condition on the surface of the representative cylinder has been applied for squirt flow (Dvorkin and Nur, 1993). Such boundary condition leads to a lower P wave velocity than Biot's theory and Gassmann equation at low frequency limit. Non-zero pressure condition has been employed by using pore pressure increment at the surface of unrelaxed fraction of pore space (Dvorkin *et al.*, 1995) to model squirt flow in fully saturated rocks. The pressure increment is related to confining pressure increment. In this way, the undrained pore rocks have relatively high frame moduli. And the predicted P wave velocity at low frequency limit is identical to Gassmann's equation.

In the case of zero pressure boundary condition ($p_m^* = 0$, $m=1, 2$), the average flow pressure \bar{p}_1 and \bar{p}_2 in the cylinder channel are determined

$$\begin{aligned} \bar{p}_1 &= \frac{1}{\pi R^2} \int_0^R 2\pi r p_1(x, r, t) dr = -\tilde{F}_1 \left(\frac{\partial U_x^{(1)}}{\partial x} - \phi_2 \frac{\partial Z_x}{\partial x} + \frac{\gamma_1}{\phi_1} \frac{\partial u_x}{\partial x} \right) \\ \bar{p}_2 &= \frac{1}{\pi R^2} \int_0^R 2\pi r p_2(x, r, t) dr = -\tilde{F}_2 \left(\frac{\partial U_x^{(2)}}{\partial x} + \phi_1 \frac{\partial Z_x}{\partial x} + \frac{\gamma_2}{\phi_2} \frac{\partial u_x}{\partial x} \right), \end{aligned} \quad (12)$$

where $\tilde{F}_m = F_m \left(1 - \frac{2J_1(\lambda_m R)}{\lambda_m R J_0(\lambda_m R)} \right)$. In the case that the pressure p in dynamic equations (5) is

approximated by its average value \bar{p} , we have wave equations in ω, k space:

$$\begin{bmatrix} a_{11}Y + b_{11} & a_{12}Y + b_{12} & a_{13}Y + b_{13} \\ a_{21}Y + b_{21} & a_{22}Y + b_{22} & a_{23}Y + b_{23} \\ a_{31}Y + b_{31} & a_{32}Y + b_{32} & a_{33}Y + b_{33} \end{bmatrix} \begin{Bmatrix} C_1 \\ C_2^{(1)} \\ C_2^{(2)} \end{Bmatrix} = 0. \quad (13)$$

where $Y = \left(\frac{k}{\omega}\right)^2$, $m=1,2$. The wave equations have nonzero solutions for constant

$C_1, C_2^{(1)}, C_2^{(2)}$ only if the determinant is zero, which provides an equation

$$AY^3 + BY^2 + CY + D = 0. \quad (14)$$

The coefficients a_{ij}, b_{ij} and A, B, C, D are given in Appendix B. This equation in $(k/\omega)^2$ has three roots, corresponding to the fast P-wave and two slow P-waves. The complex and phase P-wave velocities are defined as $v = \omega/k$, $v_p = \mathbf{Re}(v)$. The P-wave attenuation is obtained as $Q^{-1} = \mathbf{Im}(v^2) / \mathbf{Re}(v^2)$.

Discussions

BIPS reduces to BISQ in the condition of single-porosity & full-saturation

When the porous medium is composed of single porosity and fully saturated by one fluid, without loss of generality, we have $v_1 \rightarrow 1$ and $v_2 = 0, b_2 = 0, \rho_{02} = \rho_{22} = 0$. In such case, the coefficients a_{ij}, b_{ij} are

$$\begin{aligned} a_{11} &= M + \tilde{F}_1 \frac{(\alpha - \phi_{10})^2}{\phi_{10}}, & b_{11} &= -\rho_{00} + \frac{ib_1}{\omega}, \\ a_{12} &= a_{21} = \tilde{F}_1(\alpha - \phi_{10}), & b_{12} &= b_{21} = -\rho_{01} - \frac{ib_1}{\omega}, \end{aligned} \quad (15)$$

$$a_{13} = a_{31} = 0, \quad b_{13} = b_{31} = 0,$$

$$a_{22} = \tilde{F}_1 \phi_{10}, \quad b_{22} = -\rho_{11} + \frac{ib_1}{\omega},$$

$$a_{23} = a_{32} = 0, \quad b_{23} = b_{32} = 0,$$

$$a_{33} = 0, \quad b_{33} = 0.$$

Applying a linear substitution to the reduced plane wave equations we arrive at

$$\begin{bmatrix} \frac{1}{\rho_1} \left(M + \frac{\alpha \tilde{F}}{\phi} \right) Y - \frac{\rho_0}{\rho_1} & \frac{\alpha \tilde{F}}{\rho_1} Y - 1 \\ \frac{\tilde{F}}{\rho_1} Y - \frac{\rho_{01}}{\rho_1} - \frac{i \omega_c}{\omega} & \frac{\phi \tilde{F}}{\rho_1} Y - 1 + \frac{\rho_{01}}{\rho_2} + i \frac{\omega_c}{\omega} \end{bmatrix} \begin{Bmatrix} C_1 \\ C_2^{(1)} \end{Bmatrix} = 0. \quad (16)$$

Here parameter substitutions are used as $\tilde{F}_1 = \tilde{F}$, $\phi_{10} = \phi$, $b_1 = \phi_f \phi \frac{i \omega_c}{\omega}$.

The equations (16) are exactly the same as the one in BISQ model given by Dvorkin and Nur (Dvorkin and Nur, 1993) except for some trivial differences. In BISQ model, ρ_1, ρ_2 are densities related to solid and fluid respectively while here we use ρ_0 and ρ_1 . The couple density coefficient is $-\rho_a$ in BISQ model, but it is ρ_{01} here. The characteristic frequency term is $-i \frac{\omega_c}{\omega}$ in BISQ model while here is $i \frac{\omega_c}{\omega}$ in BIPS model. The opposite sign comes from that fact that we use $e^{i(\alpha x - k \cdot x)}$ in the displacements and pressures, while $e^{i(kx - \alpha t)}$ is used in BISQ model.

BIPS reduces to Biot's theory at infinity frequency

As we have shown in previous section, BIPS reduces to BISQ when porous medium is single-porosity and fully saturated by one fluid. In such case, it is easy to show that Biot theory is obtained from BIPS at infinity frequency. For uniaxial deformation in x-direction, the Biot's equations can be rewritten as

$$\begin{aligned} (A + 2N) \nabla^2 u_x + Q \nabla^2 U_x &= \frac{\partial^2}{\partial t^2} (\rho_{11} u_x + \rho_{12} U_x) + b \frac{\partial}{\partial t} (u_x - U_x) \\ Q \nabla^2 u_x + R \nabla^2 U_x &= \frac{\partial^2}{\partial t^2} (\rho_{12} u_x + \rho_{22} U_x) - b \frac{\partial}{\partial t} (u_x - U_x) \end{aligned} \quad (17)$$

In the case of $u_x = u_{x0} e^{i(\alpha x - k \cdot x)}$, $U_x = U_{x0} e^{i(\alpha x - k \cdot x)}$, a linear substitution of (17) gives

$$\begin{aligned} [(A + 2N + Q)Y - \rho_1] u_x + [(Q + R)Y - \rho_2] U_x &= 0 \\ \left(QY + \rho_a + \frac{ib}{\omega} \right) u_x + \left(RY - \rho_2 - \rho_a - \frac{ib}{\omega} \right) U_x &= 0 \end{aligned} \quad (18)$$

where $b = \mu \phi^2 / \kappa$ and $Y = (k / \omega)^2$. Here we use $\rho_1 = \rho_{11} + \rho_{12}$, $\rho_2 = \rho_{22} + \rho_{12}$ and $\rho_a = -\rho_{12}$ in the derivations. Compared with the Biot's equations given in the Appendix of the work by Dvorkin and Nur (Dvorkin and Nur, 1993)

$$\begin{aligned}
C_1 \left[Y \frac{1}{\rho_2} \left(M + \frac{\alpha \gamma F}{\phi} \right) - \frac{\rho_1}{\rho_2} \right] + C_2 \left(Y \frac{\alpha F}{\rho_2} - 1 \right) &= 0 \\
C_1 \left(Y \frac{\gamma F}{\rho_2} + \frac{\rho_a}{\rho_2} + i \frac{\omega_c}{\omega} \right) + C_2 \left(Y \frac{\phi F}{\rho_2} - 1 - \frac{\rho_a}{\rho_2} - i \frac{\omega_c}{\omega} \right) &= 0
\end{aligned} \tag{19}$$

where $\omega_c = \frac{\mu \phi}{\kappa \rho_f}$, one can easily recognize that the equations (18) and (19) are exactly the

same. The term in BISQ and Biot's equations is equivalent as

$$A + 2N + Q = M + \frac{\alpha \gamma F}{\phi}. \tag{20}$$

Dvorkin and Nur (Dvorkin and Nur, 1993) have shown that as $\omega \rightarrow \infty$, $\tilde{F} \rightarrow F$. In such case, the P wave velocity of BISQ model is identical to Biot's theory. As a consequence, the BIPS model in single-porosity fully saturated medium is degraded to BISQ model at high frequency limit, and hence is degraded to Biot's theory.

BIPS reduces to patchy saturation model at high frequency limit

For double-porosity and partially saturated medium, the BIPS model incorporates both local fluid flow and squirt flow mechanisms. As the frequency approaches infinity, the coefficients \tilde{F}_m satisfy

$$\tilde{F}_m = F_m \left(1 - \frac{2J_1(\lambda_m R)}{\lambda_m R J_0(\lambda_m R)} \right) \rightarrow F_m. \tag{21}$$

The physical meaning, as suggested by Dvorkin and Nur (Dvorkin and Nur, 1993), is clear that the fluid at high frequency limit is in unrelaxed mode and cannot be squeezed out of the pore space.

Here we will show that BIPS model degenerates to double-porosity dual-fluid patch model as the squirt flow is cancelled out at high frequency. For uniaxial deformation in x-direction, patchy model equations (Sun *et al.*, 2016) can be written as

$$\begin{aligned}
& \left[(A + 2N + Q_1 + Q_2)Y - \rho_{00} - \rho_{01} - \rho_{02} \right] u_x + \sum_{m=1}^2 \left[(Q_m + R_m)Y - \rho_{0m} - \rho_{mm} \right] U_x^{(m)} \\
& \quad + [Q_2 \phi_1 - Q_1 \phi_2 + R_2 \phi_1 - R_1 \phi_2] Y Z_x = 0 \\
& \left(Q_1 Y - \rho_{01} - \frac{ib}{\omega} \right) u_x + \left(R_1 Y - \rho_{11} + \frac{ib_1}{\omega} \right) U_x^{(1)} - R_1 Y \phi_1 Z_x = 0,
\end{aligned} \tag{22}$$

$$\left(Q_2 Y - \rho_{02} - \frac{ib}{\omega}\right)u_x + \left(R_2 Y - \rho_{22} + \frac{ib_2}{\omega}\right)U_x^{(1)} - R_2 Y \phi_2 Z_x = 0,$$

$$(\phi_2 Q_1 - \phi_1 Q_2)u_x + \phi_2 R_1 U_x^{(1)} - \phi_1 R_2 U_x^{(2)} + \left[\phi_2^2 R_1 - \phi_1^2 R_2 - (\chi_1^* \omega^2 - i\omega\beta_1^*) \frac{\phi_{10}\phi_2^2}{3} r_{10}^2\right] Z_x = 0,$$

where $Y = (k/\omega)^2$, $\chi_1^* = \left(\rho_{f_1} + \rho_{f_2} \frac{\phi_{10}}{\phi_{20}} [1 - v_1^{1/3}]\right) v_1$ and $\beta_1^* = \left(\frac{\eta_1}{\kappa_{10}} + \frac{\eta_2}{\kappa_{20}} (1 - v_1^{1/3})\right) \phi_{10} v_1$.

By substituting (12) into (5), we have the wave equations of BIPS model. After a linear substitution, the equations is written as:

$$\begin{aligned} & \left[\left(\bar{M} + \frac{\tilde{F}_1 \gamma_1^2}{\phi_1} + \frac{\tilde{F}_2 \gamma_2^2}{\phi_2} + \tilde{F}_1 \gamma_1 + \tilde{F}_2 \gamma_2 \right) Y - \rho_{00} - \rho_{01} - \rho_{02} \right] u_x + \sum_{m=1}^2 (\tilde{F}_m \gamma_m Y - \rho_{0m} - \rho_{mm}) U_x^{(m)} \\ & \quad + (\tilde{F}_2 \gamma_2 \phi_1 - \tilde{F}_1 \gamma_1 \phi_2 + \tilde{F}_2 \phi_2 \phi_1 - \tilde{F}_1 \phi_1 \phi_2) Y Z_x = 0, \\ & \left[\gamma_1 \tilde{F}_1 Y - \rho_{01} - \frac{ib_1}{\omega} \right] u_x + \left[\phi_1 \tilde{F}_1 Y - \rho_{11} + \frac{ib_1}{\omega} \right] U_x^{(1)} - \phi_1 \phi_2 \tilde{F}_1 Y Z_x = 0, \\ & \left[\gamma_2 \tilde{F}_2 Y - \rho_{02} - \frac{ib_2}{\omega} \right] u_x + \left[\phi_2 \tilde{F}_2 Y - \rho_{22} + \frac{ib_2}{\omega} \right] U_x^{(2)} + \phi_1 \phi_2 \tilde{F}_2 Y Z_x = 0, \\ & (\phi_1 \gamma_2 \tilde{F}_2 - \phi_2 \gamma_1 \tilde{F}_1) u_x - \phi_1 \phi_2 \tilde{F}_1 U_x^{(1)} + \phi_1 \phi_2 \tilde{F}_2 U_x^{(2)} + \left[(\chi_1 \omega^2 - i\beta_1 \omega) \frac{\phi_1 \phi_2^2}{3} + \phi_1 \phi_2^2 \tilde{F}_1 + \phi_1^2 \phi_2 \tilde{F}_2 \right] Z_x = 0. \end{aligned} \quad (23)$$

It is clear that when $\omega \rightarrow \infty$, we have $\tilde{F}_m \rightarrow F_m$. We will not show the details here, but it is not difficult to derive following relations for BIPS and patchy models:

$$A + 2N = \bar{M} + \frac{F_1 \gamma_1^2}{\phi_1} + \frac{F_2 \gamma_2^2}{\phi_2}, \quad (24)$$

$$Q_1 = F_1 \gamma_1, \quad Q_2 = F_2 \gamma_2, \quad (25)$$

$$R_1 = F_1 \phi_1, \quad R_2 = F_2 \phi_2. \quad (26)$$

The terms before $u_x, U_x^{(1)}, U_x^{(2)}$ and Z_x in (22) and (23) are equivalent to each other. As a consequence, at the high frequency limit, the BIPS model is degraded to patchy model. Please note that the patch size r_{10} appear in TLP model. But in BIPS model, the patch size obeys a random distribution, rather than a single predefined value. In such a way, BIPS model will not explicitly depends on patch size r_{10} , which is usually a trouble to determine in experiment.

Numerical examples

The dispersion and attenuation of P-waves propagating in porous medium depends on fluid density, modulus, viscosity as well as skeleton properties (such as bulk modulus, density and

permeability). In BISQ model, the characteristic squirt length R is another important parameter. The illustration of effects of permeability and characteristic squirt length on P wave velocities have been given by Dvorkin and Nur (Dvorkin and Nur, 1993). In BIPS model, P wave velocity depends on not only the rock physics parameters of the double-porosity matrix, but also the parameters of fluid patches. In addition, the fluid patch volume fraction in BIPS model is an extra parameter as important as characteristic squirt length in BISQ model. In this section, we will investigate the effects of permeability, viscosity, patch volume fractions and characteristic squirt length on P wave dispersion and attenuation.

The effects of frequency and fluid type

Firstly, we investigate the effects of frequency and fluid type on P wave velocity dispersion and attenuation. The rock physics parameters are from the numerical examples in work of Dvorkin and Nur (Dvorkin and Nur, 1993). The porosity is 0.15. The bulk modulus and Poisson's ratio of matrix are $K = 16$ GPa and 0.15. The modulus and density of solid phase are $K_s = 38$ GPa and 2650 kg/m^3 . The velocity vs frequency curves are calculated by BIPS model and compared with Biot's theory, Gassmann equation, BISQ and TLP model (Figure 2).

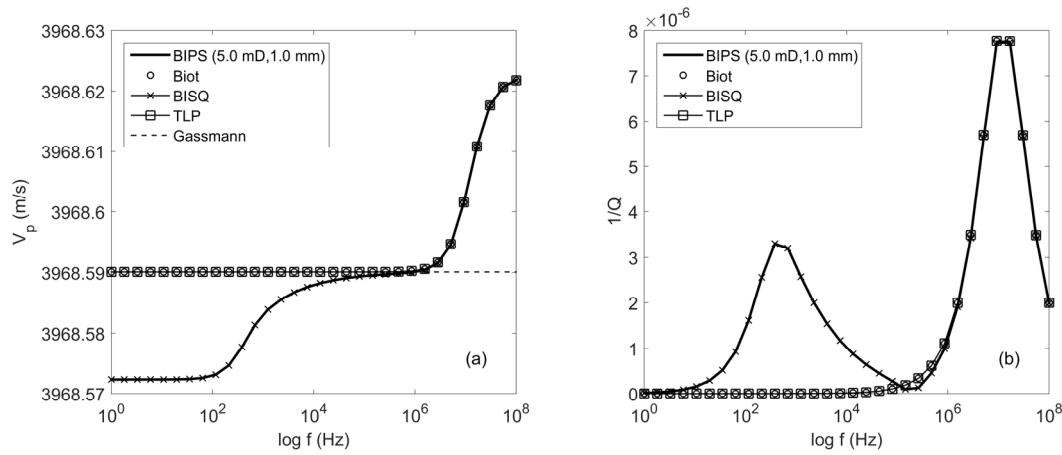


Figure 2 Prediction of P-wave velocity dispersion (a) and attenuation (b) by BIPS, BISQ, TLP, Biot and Gassmann methods. The volume fraction of inner fluid pocket (gas) is 1. The overall matrix has uniform porosity.

In the first case, the fluid in the inner pocket is gas (modulus $K_{gas} = 0.142$ MPa, density $\rho_{gas} = 1.2 \text{ kg/m}^3$, viscosity $\eta_{gas} = 18.6 \text{ } \mu\text{Pa}\cdot\text{s}$). The surrounding fluid is water (modulus $K_{water} = 2.2$ GPa, density $\rho_{water} = 1000 \text{ kg/m}^3$, viscosity $\eta_{water} = 1.0 \text{ mPa}\cdot\text{s}$). The volume fraction of inner gas pocket is set to 1, i.e., the matrix is fully saturated by gas.

The results in Figure 2 give following features. (1) The squirt flow effect is switch off at high frequency limit, i.e., $\tilde{F} \rightarrow F$, the velocities dispersion (Figure 2 (a)) and attenuation (Figure 2 (b)) of BIPS model match very well to that of Biot's theory. (2) The velocities of BIPS and BISQ models at low frequency are a little bit lower than Biot's theory (Figure 2 (a)), but the difference is extremely tiny in full gas saturation case (around 3968.57m/s to 3968.59m/s). (3) The predicted dispersion and attenuation by TLP model overlap with Biot's theory very well. The reason is that TLP model incorporates Biot's mechanism and local fluid flow at fluid interfaces simultaneously. In the fully gas saturation case, there is only one fluid and the LFIF effect at patch interface disappear. Thus TLP model degenerates to Biot's theory. (4)It is clear that BIPS and BISQ models has two attenuation peaks (Figure 2 (b)). The peak at high frequency (between 1MHz and 100MHz) is related to Biot mechanism, which overlaps perfectly with the curve of Biot's theory. The peak at lower frequency (between 100Hz and 10KHz) is caused by the squirt effect, which has been taken into consideration in BIPS and BISQ models.

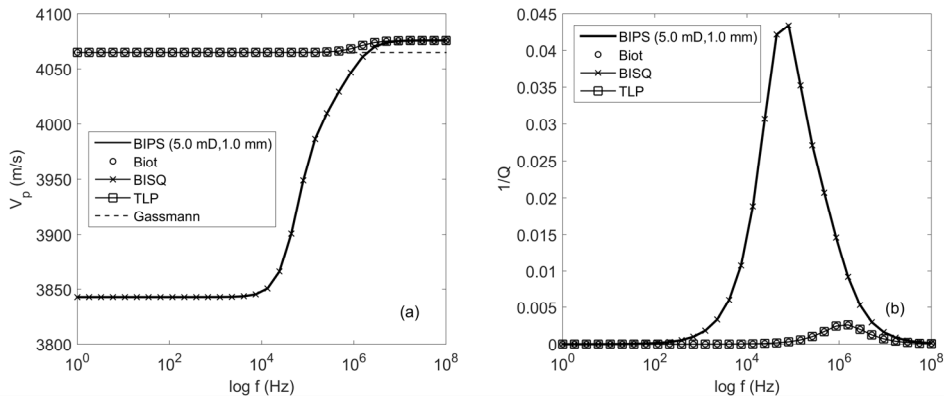


Figure 3 Prediction of P-wave velocity dispersion (a) and attenuation (b) by BIPS, BISQ, TLP, Biot and Gassmann methods. The volume fraction of inner fluid pocket (water) is 1. The overall matrix has uniform porosity.

In the second case, the inner pocket is filled with water and the surrounding fluid is gas. The volume fraction of water pocket is set to 1, i.e., the matrix is fully saturated by water. The velocity dispersion and attenuation are shown in Figure 3. The water-saturated case shows consistent behaviors as observed in the gas-saturated case. In addition, we underline that squirt flow effect are apparently enhanced in water-saturation case. It should be noted that: (1) the velocities of BIPS and BISQ at low frequency are substantially lower than that of Biot's theory. The velocity difference has been attributed to the constant pressure boundary condition(Dvorkin and Nur, 1993). (2) The two attenuation peaks of BIPS and BISQ models,

i.e., the squirt peak at low frequency and Biot peak at high frequency, move towards each other and combine into a single larger peak. The Biot peaks of TLP model and Biot's theory are still there, but shift towards lower frequency.

It should be noted that the movement of attenuation peak along frequency axis depends not only on fluid mobility (viscosity and permeability), but also on fluid density and bulk modulus. It has been observed that as the viscosity of pore fluid increase, or matrix permeability decrease, the attenuation peak of squirt mechanism shifts lower frequency (Dvorkin *et al.*, 1994). The TLP peaks move in the same direction as squirt model. On the other hand, Biot peak shifts in the opposite direction. Here we can find that as gas-saturation transits to water-saturation, the fluid viscosity increases from $\eta_{gas} = 18.6 \mu\text{Pa}\cdot\text{s}$ to $\eta_{water} = 1.0 \text{ mPa}\cdot\text{s}$. The attenuation peak is supposed to shift towards low frequency since the fluid mobility decrease as viscosity increase. Surprisingly, the squirt peak and TLP peak shift to higher frequency region. The reason of this discrepancy comes from the fact that the fluid modulus increase from $K_{gas} = 0.142 \text{ MPa}$ to $K_{water} = 2.2 \text{ GPa}$ and density increase from $\rho_{gas} = 1.2 \text{ kg/m}^3$ to $\rho_{water} = 1000 \text{ kg/m}^3$. In summary, in single-fluid saturation case, the patch effect disappears and BIPS model is the same as BISQ model. BIPS and BISQ model contain both squirt and Biot attenuation peaks. When the fluid changes from gas to water, the squirt effect is substantially enhanced. In addition, attenuation peaks caused by squirt and Biot mechanisms move towards each other and combine into a large peak when the matrix is fully saturated by water. Shift towards higher frequency is the property of Biot's theory. This might be the reason of the shift direction you observe.

The effects of patch saturation and permeability

In this section, we investigate the effects of patch saturation and permeability on P wave velocity dispersion and attenuation. The inner fluid pockets are filled with water in the calculation by BIPS and TLP models. The pocket volume fraction is set to 0.9 (Figure 4) and 0.3 (Figure 5) respectively to check the influence of patch saturation. In velocity prediction by Biot's theory and BISQ model, the matrix is saturated by water. The rock physics parameters are the same as in previous section. BISQ characteristic radius is set to 1mm here.

To find out the underlying reasons causing the velocity difference among BIPS, BISQ and TLP models, we plot the dispersion/attenuation figure against frequency in Figure 4 and Figure 5. The results show following apparent features. (1) In partial saturation case, the TLP velocity is much lower than Biot and Gassmann velocity at low frequency, rather than overlap

with Biot’s theory as in full-saturation case. The reason of the velocity decrease is that an interface emerges between inner water pocket and surround gas patch. The patch effect in TLP model arises from the LFIF at the interface and cause the velocity decrease remarkably. (2)As one can see in Figure 4 (b) and Figure 5 (b), BIPS, BISQ, TLP and Biot attenuation peaks have difference heights and locations. As volume fraction of inner water pocket decrease from 0.9 to 0.3 (Figure 5 (b)), the BIPS and TLP peaks are dwarfed. While BISQ and Biot peaks do not change. The physical meaning of this sharp change in peak height is that as the pocket fluid decrease, the kinetic energy dissipation caused by patchy mechanism in BIPS and TLP models is weakened. (3) It is clear that BIPS peak has a bump near the location of Biot peak (Figure 4 (b) and Figure 5 (b)), which indicates that BIPS model includes the effect of Biot mechanism. (4) An interesting observation is that BIPS peak is lower than TLP peak (Figure 4 (b) and Figure 5 (b)). In current partial-saturation case, BIPS model includes Biot, patchy and squirt mechanism simultaneously. A reasonable explanation that patchy-saturation effect can be weakened by squirt flow effect. The LFIF dissipation at the patch interface is to be partially cancelled by the existence of squirt flow, which has been suggested by Johnson(Johnson, 2001).

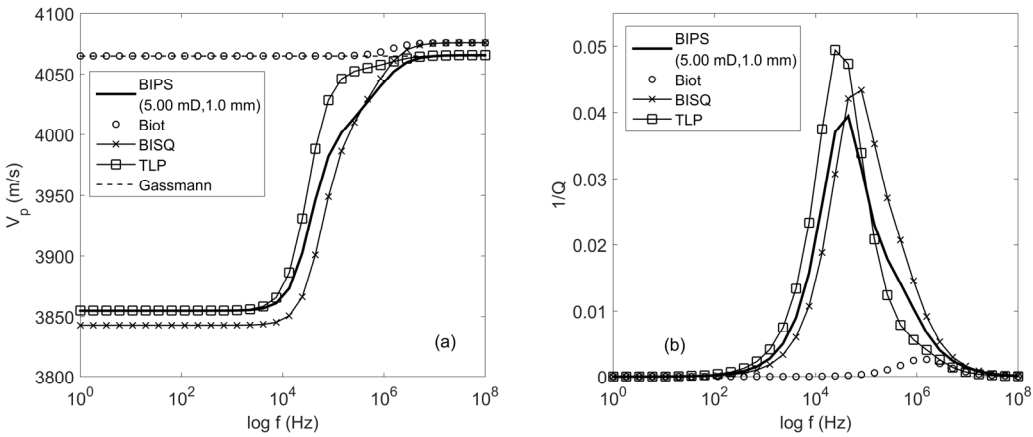


Figure 4 Prediction of P-wave velocity dispersion (a) and attenuation (b) by BIPS, BISQ, TLP, Biot and Gassmann methods. The volume fraction of inner fluid pocket (water) is 0.9. The permeability is 5mD. The squirt characteristic length is 1mm.

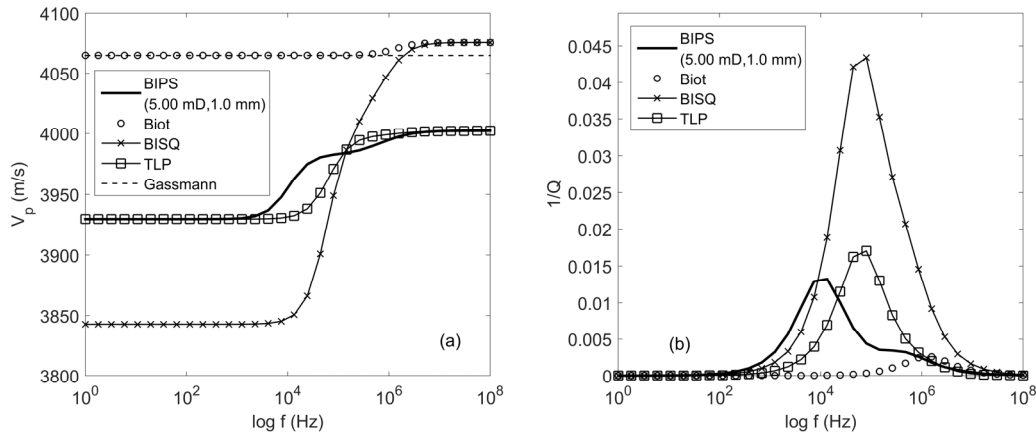


Figure 5 Prediction of P-wave velocity dispersion (a) and attenuation (b) by BIPS, BISQ, TLP, Biot and Gassmann methods. The volume fraction of inner fluid pocket (water) is 0.3. The permeability is 5mD. The squirt characteristic length is 1mm.

As we have shown above, LFIF and squirt flow are identified as separate mechanisms by comprehensive analysis of frequency, fluid type and fluid pocket size. Moreover, we find that the key difference and coupling effects between patchy and squirt effects are in form of attenuation peak variation as the whole concentric patch size changes. To facilitate the understating of the relation between BIPS, BISQ and TLP model, the whole patch (including the inner pocket and surrounding fluid patch) size is set to 0.1mm and 5mm respectively. The results are shown in Figure 6 and Figure 7.

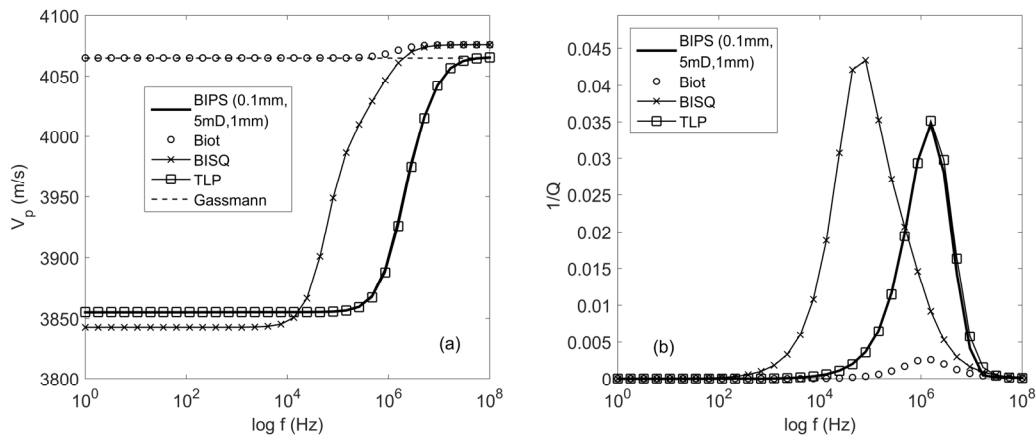


Figure 6 Prediction of P-wave velocity dispersion (a) and attenuation (b) by BIPS, BISQ, TLP, Biot and Gassmann methods. The volume fraction of inner fluid pocket (water) is 0.9. The permeability is 5mD. The squirt characteristic length is 1mm. The whole patch size is 0.1 mm.

As shown in Figure 6 (b), the attenuation peaks of BIPS and TLP, which are located at high frequency region (around 1MHz), are at the right hand side of BISQ peak. Moreover, BIPS and TLP peaks overlap with each other quite well, suggesting that BIPS is degraded to TLP at high frequency limit, which has been theoretically analyzed in Discussions section.

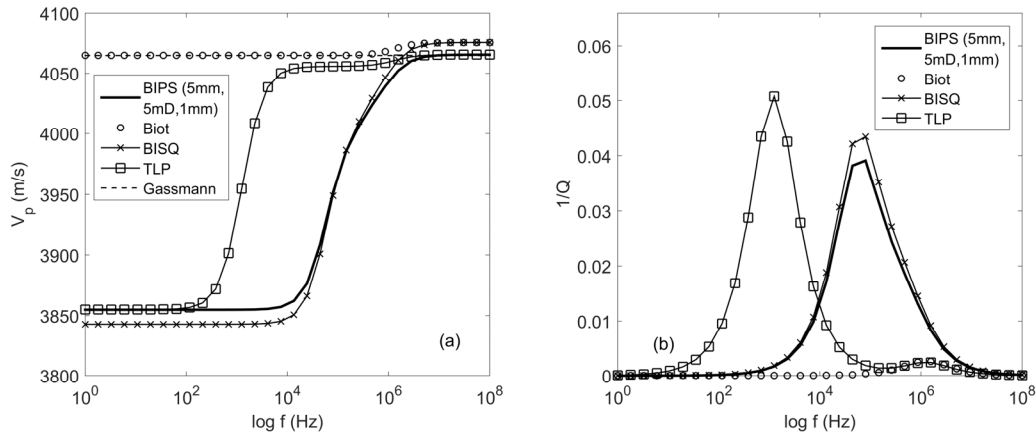


Figure 7 Prediction of P-wave velocity dispersion (a) and attenuation (b) by BIPS, BISQ, TLP, Biot and Gassmann methods. The volume fraction of inner fluid pocket (water) is 0.9. The permeability is 5mD. The squirt characteristic length is 1mm. The whole patch size is 5 mm.

As the whole patch size increases to 5mm, the TLP peak has a remarkable shift to lower frequency (around 1kHz) (Figure 7 (b)). Correspondingly, the P-wave velocity increase lot for the same frequency (Figure 7 (a)). The physical explanation underline this velocity enhancement is that larger characteristic patchy size, which indicates larger fluid heterogeneity, requires much longer time for the fluid to relax. The ratio between mesoscopic fluid patch size and diffusion length is of great importance for patchy mechanism. It describes the velocity dispersion caused by LFIF between inner fluid pocket and surrounding fluid patch. Since the fluids have no enough time to relax in larger patches, the porous rock is actually in an unrelaxed state.

Surprisingly, we find that there is no BIPS peak at low frequency. As we have demonstrated above, BIPS is a unified model that incorporates the three most important mechanisms: Biot mechanism, patchy saturation mechanism and squirt mechanism. The patchy saturation mechanism, which has also been incorporated in TLP model, gives the attenuation peak shift towards low frequency. However, the effect of patchy saturation, i.e., a shift of attenuation peak to low frequency, does not appear in BIPS model. More importantly, BIPS peak overlaps the BISQ peak pretty well, except for a reduction in peak height. A reasonable interpretation is that squirt flow mechanism suppresses the patchy saturation effects to a great extent and trim the patchy saturation peak completely, which has been demonstrated in Figure 4 (b), Figure 5 (b) and also in other works(Johnson, 2001, Tserkovnyak and Johnson, 2002).

In addition to patch size effect, we explore the dependence of velocity dispersion/attenuation on permeability. As the matrix permeability is reduced from 5mD (Figure 4) to 0.1mD (Figure 8), the sharp velocity transition region and attenuation peaks of BIPS, BISQ and TLP

models shift towards low frequency (Figure 8). Whereas the Biot peak exhibits the opposite behavior. The physical meaning of this disparity has been attributed to the difference between Biot mechanism and squirt-flow mechanism (Dvorkin *et al.*, 1994). It is obvious that the relative position and heights of BIPS, BISQ and TLP peaks do not have apparent changes (Figure 8 (b)), which is consistent at different permeability.

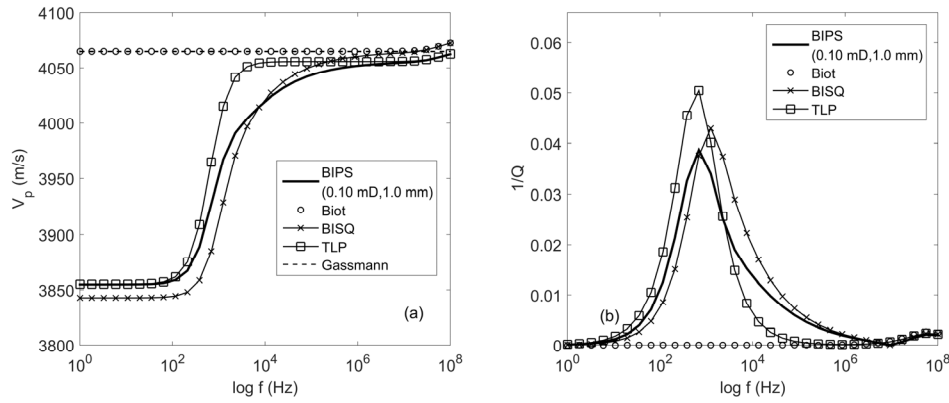


Figure 8 Prediction of P-wave velocity dispersion (a) and attenuation (b) by BIPS, BISQ, TLP, Biot and Gassmann methods. The volume fraction of inner fluid pocket (water) is 0.9. The permeability is 0.1mD. The squirt characteristic length is 1mm.

The present analysis clearly demonstrates the remarkable difference of dispersion/attenuation mechanism among Biot's theory, BISQ model and patchy models. As one can see, TLP model and Biot theory are the same in full saturation case since the interface LFIF effect of TLP model is cancelled. At the same time, BIPS model reduces to BISQ model for the reason that only Biot mechanism and squirt mechanism are retained for BIPS in full saturation case. It's obviously that in partial-saturation case BIPS model persists all the three (Biot-patchy-squirt) mechanisms. Whereas BISQ model contains the Biot-squirt mechanism and TLP model incorporates the Biot-patchy mechanism. The effects of frequency, inner pocket fluid and permeability on peaks of different mechanism show distinctive characteristics, which strongly indicate that the Biot, patchy and squirt mechanisms are three fundamental physical processes that dominate the wave propagations in partially saturated double-porosity media. Any one of the three mechanism along does not provide adequate interpretations of the dispersion and attenuation in natural rocks.

In summary, Biot, patchy and squirt mechanisms are distinguishable from each other. In addition, they also share common parts and couple with each other. These results, taken with the fact that matrix and fluid inhomogeneity is a quite typical phenomenon in natural rocks, indicate that the BIPS model can be regarded as novel unified model to predict realistic dispersion and attenuation in reservoir rocks.

Experimental evidence of squirt flow and LFIF flow in sandstone

Subramaniyan and Quintal et al (Subramaniyan *et al.*, 2015b) reported the evidence of squirt flow in Fontainebleau sandstone through laboratory observation of seismic attenuation. A Fontainebleau sandstone (porosity 8% and permeability 12mD) was saturated with glycerin-water mixture of varying viscosity (thus varying volume fraction of glycerin in the mixture). The Young's module attenuations were measured at the confining pressures of 5, 10 and 15 MPa. As the viscosity of the saturating fluid decrease (thus glycerin fraction decrease in the mixture), the attenuation magnitude drops and the peak frequency shifts to higher frequencies. The attenuation peak frequency is inversely proportional to fluid viscosity, which is a result of squirt flow (Subramaniyan *et al.*, 2015a).

The squirt flow, patch saturation and global fluid flow mechanism are clearly related, but in a way that is not always obvious. The attenuation peak frequency of patch saturation model has the similar behavior as squirt flow, i.e., it is also inversely proportional to viscosity. Identifying the cause of inverse proportion effect is crucial to the understanding of BIPS model.

We believe that two main causes of attenuation at low pressure are: (1) LFIF at patch interface; (2) squirt flow between compliant and stiff pore. At the high pressure, all the compliant pores in the sandstone are assumed to be closed. Thus, the squirt flow effect will also cease. For glycerin-water mixture saturation, if attenuation magnitude drops and peak frequency shifts inversely proportional to fluid viscosity, the attenuation is no doubt caused by patch saturation.

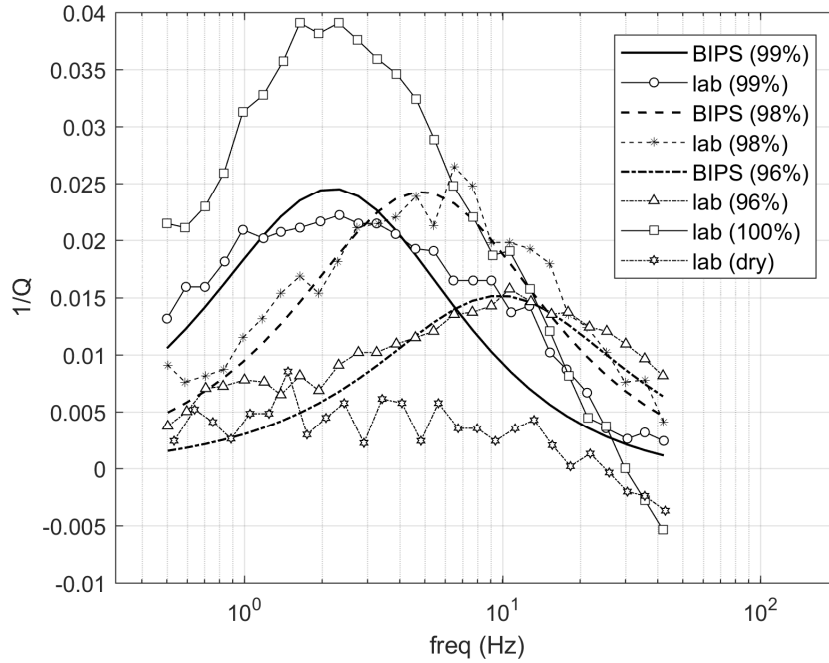


Figure 9 Attenuation for confining pressures of 15 MPa in Berea sandstone. The water saturation, ranging from dry conditions to around 100%. BIPS model prediction and the experiment data are shown in different lines.

The Subramanian et al. gave the attenuation at high pressure (15 MPa) in sandstone for glycerin full saturation (Subramanian *et al.*, 2015a). In such case, there exists no patch interface and LFIF effect can not be identified. Fortunately, the attenuations in partially saturated Berea sandstone at high pressure (15MPa) have been reported recently (Chapman *et al.*, 2016), which is caused by LFIF, rather than squirt flow. The Berea sandstone has a porosity of 18% and a permeability of 50mD. Solid grain density is 2650 kg/m³. Bulk modulus of solid grains is 36 GPa. Bulk and shear modulus of dry frame are 15.1 GPa and 14 GPa (at confining pressure 25 MPa). Bulk modulus, density and viscosity of water are 2.2 GPa, 1000 kg/m³ and 0.001 Pa.s. Bulk modulus, density and viscosity of air are 0.1 MPa, 1kg/m³ and 2×10⁻⁵ Pa.s. The sandstone is fully saturated with water firstly. Then water saturation decreases to lower percentages. At confining pressure of 15MPa, the extensional-mode attenuation magnitude were measured for 96%, 98%, 99% and 100% water saturation (Figure 9). Attenuation decreases and the peak shifts to higher frequency as water saturation decrease from nearly 100% to 96%. Full water saturation indicates there is only one uniform fluid in pore space. As water saturation decreases, air patches appear and increase gradually. LFIF becomes more and more important as water-air interface expands.

Here we predict attenuation by BIPS model and compare the results with laboratory data (Figure 9). Since the attenuations were measured at high confining pressure, compliant

pore/cracks remain closed during the measurements. Thus, squirt flow effect is absent in the attenuation. The experiment data and predicted results show clearly that the peak frequency is inversely proportional to water saturation (from 100% to 96%), which is an evidence of LFIF. This phenomenon has also been observed in numerical example in Figure 4(b) and Figure 5(b).

The results show that the BIPS model allow us to reproduce the attenuation-frequency relation observed in laboratory. Predicted attenuations exhibit the same dependence on water saturation as experiment data. It is important to recall that patch size must be considered as a function of saturation. Although patch radius is hardly to be measured directly, it can be estimated by matching the calculated velocity with experiment data. Indeed, the patch radii have been estimated based on the four-term polynomial formula with coefficients(Liu *et al.*, 2016). Even though mechanism of how the fluid patch evolves in porous media is still poorly understood, the application of quantitative function between patch radius and saturation in this study is expected to shed light on the remarkable role of partial-saturation in affecting wave propagations.

Conclusions

We present a Biot-patchy-squirt (BIPS) method to derive wave equations in partially saturated double-porosity medium. Wave dispersion and attenuation are formulated. The importance of current work is twofold. (1) BIPS model combines macroscopic Biot flow, mesoscopic patchy heterogeneities and microscopic squirt effect. This model provides a possibility to investigate the key information about the coupling among global flow, local fluid flow and squirt flow. (2) BIPS model incorporates both fluid and solid heterogeneities in porous media, which is commonly observed in natural reservoir rocks. The BIPS is a more general model and can reduce to Biot's theory, BISQ model and TLP model in limiting cases. A comprehensive analysis of the effects of frequency, fluid type, patch saturation and permeability by numerical examples reveal that Biot, patchy and squirt mechanisms are distinct from each other. In addition, they also couple with each other. The LFIF dissipation at the patch interface is to be partially cancelled by the existence of squirt flow. We conclude that in fractured and partially saturated rock, any single mechanism is not sufficient and the combined effects have evident effects on attenuation. The agreement between the predicted attenuation and experiment data in sandstone confirms the agreement between the BIPS model and naturally occurred phenomenon. The new method may actually bring much broader understandings for the study of wave phenomena in partially saturated heterogeneous media.

Funding

The research was supported by the National Natural Science Foundation of China (Grant no. 41874137, Grant no. 42074144), and National Key R & D Program of China (2018YFA0702501)

References

- Aifantis, E.C., 1977. Introducing a multi-porous medium. Proceedings of the 15th midwestern mechanics conference, *Developments in Mechanics*, 8, 209-211.
- Aifantis, E.C., 1979. A new interpretation of diffusion in high-diffusivity paths—a continuum approach, *Acta Metallurgica*, 27, 683-691.
- Aifantis, E.C., 1980. On the problem of diffusion in solids, *Acta Mechanica*, 37, 265-296.
- Ali, A. & Jakobsen, M., 2014. On the relative importance of global and squirt flow in cracked porous media, *Acta Geodaetica et Geophysica*, 49, 105-123.
- Ba, J., Carcione, J.M. & Nie, J.X., 2011. Biot-Rayleigh theory of wave propagation in double-porosity media, *Journal of Geophysical Research*, 116, B06202.
- Ba, J., Carcione, J.M. & Sun, W.T., 2015. Seismic attenuation due to heterogeneities of rock fabric and fluid distribution, *Geophys J Int*, 202, 1843-1847.
- Bacri, J.-C. & Salin, D., 1986. Sound velocity of a sandstone with oil and brine at different concentrations, *GEOPHYSICAL RESEARCH LETTERS*, 13, 326-328.
- Bai, M., 1999. On equivalence of dual-porosity poroelastic parameters, *Journal of Geophysical Research: Solid Earth*, 104, 10461-10466.
- Bai, M., Elsworth, D. & Roegiers, J.C., 1993. Modeling of naturally fractured reservoirs using deformation dependent flow mechanism, *International Journal of Rock Mechanics and Mining Sciences & Geomechanics Abstracts*, 30, 1185-1191.
- Barenblatt, G.I., Zheltov, I.P. & Kochina, I.N., 1960. Basic concepts in the theory of seepage of homogeneous liquids in fissured rocks [strata], *Journal of Applied Mathematics and Mechanics*, 24, 1286-1303.
- Berryman, J.G. & Pride, S.R., 2005. Dispersion of waves in porous cylinders with patchy saturation: Formulation and torsional waves, *The Journal of the Acoustical Society of America*, 117, 1785-1795.
- Berryman, J.G. & Wang, H.F., 1995. The elastic coefficients of double-porosity models for fluid transport in jointed rock, *J Geophys Res-Sol Ea*, 100, 24611-24627.
- Berryman, J.G. & Wang, H.F., 2000. Elastic wave propagation and attenuation in a double-porosity dual-permeability medium, *Int J Rock Mech Min*, 37, 63-78.
- Biot, M.A., 1941. General Theory of Three - Dimensional Consolidation, *J Appl Phys*, 12, 155-164.
- Biot, M.A., 1956. Theory of Propagation of Elastic Waves in a Fluid-Saturated Porous Solid .1. Low-Frequency Range, *J Acoust Soc Am*, 28, 168-178.
- Biot, M.A., 1962. Mechanics of Deformation and Acoustic Propagation in Porous Media, *J Appl Phys*, 33, 1482-1498.
- Cadoret, T., Marion, D. & Zinszner, B., 1995. Influence of frequency and fluid distribution on elastic wave velocities in partially saturated limestones, *Journal of Geophysical Research: Solid Earth*, 100, 9789-9803.
- Cadoret, T., Mavko, G. & Zinszner, B., 1998. Fluid distribution effect on sonic attenuation in partially saturated limestones, *Geophysics*, 63, 154-160.
- Carcione, J.M. & Picotti, S., 2006. P-wave seismic attenuation by slow-wave diffusion: Effects of inhomogeneous rock properties, *Geophysics*, 71, O1–O8.
- Chapman, M., Zatsepin, S.V. & Crampin, S., 2002. Derivation of a microstructural poroelastic model, *Geophys J Int*, 151, 427-451.
- Chapman, S., Tisato, N., Quintal, B. & Holliger, K., 2016. Seismic attenuation in partially saturated Berea sandstone submitted to a range of confining pressures, *Journal of Geophysical Research: Solid Earth*, 121, 1664-1676.

- Dutta, N.C. & Ode, H., 1979. Attenuation and Dispersion of Compressional Waves in Fluid-Filled Porous Rocks with Partial Gas Saturation (White Model) .1. Biot Theory, *Geophysics*, 44, 1777-1788.
- Dutta, N.C. & Odé, H., 1979. Attenuation and Dispersion of Compressional Waves in Fluid-Filled Porous Rocks with Partial Gas Saturation (White Model) .2. Results, *Geophysics*, 44, 1789-1805.
- Dutta, N.C. & Seriff, A.J., 1979. On White's model of attenuation in rocks with partial gas saturation, *Geophysics*, 44, 1806-1812.
- Dvorkin, J., Mavko, G. & Nur, A., 1995. Squirt Flow in Fully Saturated Rocks, *Geophysics*, 60, 97-107.
- Dvorkin, J., Nolen-Hoeksema, R.C. & Nur, A., 1994. The squirt-flow mechanism; macroscopic description, *Geophysics*, 59, 428.
- Dvorkin, J. & Nur, A., 1993. Dynamic poroelasticity: A unified model with the squirt and the Biot mechanisms, *Geophysics*, 58, 524-533.
- Elsworth, D. & Bai, M., 1992. Flow - Deformation Response of Dual - Porosity Media, *Journal of Geotechnical Engineering*, 118, 107-124.
- Gregory, A., 1976. FLUID SATURATION EFFECTS ON DYNAMIC ELASTIC PROPERTIES OF SEDIMENTARY ROCKS, *Geophysics*, 41, 895-921.
- Gurevich, B., Makarynska, D., de Paula, O. & Pervukhina, M., 2010. A simple model for squirt-flow dispersion and attenuation in fluid-saturated granular rocks, *Geophysics*, 75, N109-N120.
- Helle, H.B., Pham, N.H. & Carcione, J.M., 2003. Velocity and attenuation in partially saturated rocks: poroelastic numerical experiments, *Geophysical Prospecting*, 51, 551-566.
- Johnson, D.L., 2001. Theory of frequency dependent acoustics in patchy-saturated porous media, *J Acoust Soc Am*, 110, 682-694.
- Khaled, M.Y., Beskos, D.E. & Aifantis, E.C., 1984. On the theory of consolidation with double porosity—III A finite element formulation, *International Journal for Numerical and Analytical Methods in Geomechanics*, 8, 101-123.
- Lebedev, M., Toms-Stewart, J., Clennell, B., Pervukhina, M., Shulakova, V., Paterson, L., Gurevich, B. & Wenzlau, F., 2009. Direct laboratory observation of patchy saturation and its effects on ultrasonic velocities, *The Leading Edge*, 28, 24-27.
- Liu, J., Müller, T.M., Qi, Q., Lebedev, M. & Sun, W., 2016. Velocity-saturation relation in partially saturated rocks: Modelling the effect of injection rate changes, *Geophysical Prospecting*, 64, 1054-1066.
- Lopes, S. & Lebedev, M., 2012. Research note: Laboratory study of the influence of changing the injection rate on the geometry of the fluid front and on P-wave ultrasonic velocities in sandstone, *Geophysical Prospecting*, 60, 572-580.
- Lopes, S., Lebedev, M., Müller, T.M., Clennell, M.B. & Gurevich, B., 2014. Forced imbibition into a limestone: measuring P-wave velocity and water saturation dependence on injection rate, *Geophysical Prospecting*, 62, 1126-1142.
- Marketos, G. & Best, A.I., 2010. Application of the BISQ model to clay squirt flow in reservoir sandstones, *Journal of Geophysical Research: Solid Earth*, 115, n/a-n/a.
- Mavko, G. & Nur, A., 1975. Melt squirt in the asthenosphere, *Journal of Geophysical Research*, 80, 1444-1448.
- Mavko, G.M. & Nur, A., 1979. Wave Attenuation in Partially Saturated Rocks, *Geophysics*, 44, 161-178.
- Müller, T. & Gurevich, B., 2004. One - dimensional random patchy saturation model for velocity and attenuation in porous rocks, *Geophysics*, 69, 1166-1172.

- Müller, T.M., Toms-Stewart, J. & Wenzlau, F., 2008. Velocity-saturation relation for partially saturated rocks with fractal pore fluid distribution, *Geophysical Research Letters*, 35, L09306.
- Murphy, W.F., 1984. Acoustic measures of partial gas saturation in tight sandstones, *Journal of Geophysical Research* 89, 11549–11559.
- Norris, A.N., 1993. Low - frequency dispersion and attenuation in partially saturated rocks, *The Journal of the Acoustical Society of America* 94, 359-370.
- Oconnell, R.J. & Budiansky, B., 1977. Viscoelastic Properties of Fluid-Saturated Cracked Solids, *Journal of Geophysical Research*, 82, 5719-5735.
- Pride, S.R., Berryman, J.G. & Harris, J.M., 2004. Seismic attenuation due to wave-induced flow, *Journal of Geophysical Research*, 109, B01201.
- Rubino, J.G. & Holliger, K., 2012. Seismic attenuation and velocity dispersion in heterogeneous partially saturated porous rocks, *Geophys J Int*, 188, 1088-1102.
- Sams, M.S., Neep, J.P., Worthington, M.H. & King, M.S., 1997. The measurement of velocity dispersion and frequency-dependent intrinsic attenuation in sedimentary rocks, *Geophysics*, 62, 1456-1464.
- Sharma, M.D., 2017. Wave propagation in double-porosity dual-permeability materials: Velocity and attenuation, *Advances in Water Resources*, 106, 132-143.
- Subramaniyan, S., Madonna, C., Quintal, B. & Saenger, E., 2015a. Laboratory-based seismic attenuation in Fontainebleau sandstone: Evidence of squirt flow. in *SEG Technical Program Expanded Abstracts 2015*, pp. 3111-3115 Society of Exploration Geophysicists.
- Subramaniyan, S., Quintal, B., Madonna, C. & Saenger, E.H., 2015b. Laboratory-based seismic attenuation in Fontainebleau sandstone: Evidence of squirt flow, *Journal of Geophysical Research: Solid Earth*, 120, 7526-7535.
- Sun, W., 2018. Petrophysical model of partially saturated complex pore reservoir and its application. in *Research report of CNPC Research Institute of Science and Technology*, Tsinghua University Beijing, China.
- Sun, W., Ba, J. & Carcione, J.e.M., 2016. Theory of wave propagation in partially saturated double-porosity rocks: a triple-layer patchy model, *Geophys J Int*, 205, 22-37.
- Sun, W., Ba, J., Müller, T.M., Carcione, J.M. & Cao, H., 2015. Comparison of P-wave attenuation models of wave-induced flow, *Geophysical Prospecting*, 63, 378-390.
- Terzaghi, K., 1943. *Theoretical soil mechanics*, edn, Vol., pp. Pages, John Wiley & Sons, New York.
- Thas, K., 2007. Can one hear the shape of a Lie-type geometry, *Inverse Probl*, 23, 2021-2028.
- Toms-Stewart, J., Müller, T., Gurevich, B. & Paterson, L., 2009. Statistical characterization of gas-patch distributions in partially saturated rocks, *Geophysics*, 74, WA51-WA64.
- Toms, J., Müller, T.M., Ciz, R. & Gurevich, B., 2006. Comparative review of theoretical models for elastic wave attenuation and dispersion in partially saturated rocks, *Soil Dynamics and Earthquake Engineering*, 26, 548-565.
- Toms, J., Müller, T.M. & Gurevich, B., 2007. Seismic attenuation in porous rocks with random patchy saturation, *Geophysical Prospecting*, 55, 671-678.
- Tserkovnyak, Y. & Johnson, D.L., 2002. Can one hear the shape of a saturation patch, *GEOPHYSICAL RESEARCH LETTERS*, 29, 1108.
- White, J.E., 1975. Computed Seismic Speeds and Attenuation in Rocks with Partial Gas Saturation, *Geophysics*, 40, 224-232.
- White, J.E., Mikhaylova, N.G. & Lyakhovitskiy, F.M., 1975. Low-frequency seismic waves in fluid-saturated layered rocks, *The Journal of the Acoustical Society of America*, 57, 654-659.

- Wilson, R.K. & Aifantis, E.C., 1982. On the theory of consolidation with double porosity, *International Journal of Engineering Science*, 20, 1009-1035.
- Winkler, K.W., 1985. Dispersion analysis of velocity and attenuation in Berea sandstone, *Journal of Geophysical Research: Solid Earth*, 90, 6793-6800.
- Winkler, K.W., 1986. Estimates of velocity dispersion between seismic and ultrasonic frequencies, *Geophysics*, 51, 183-189.
- Wyllie, M., Gregory, A. & Gardner, G., 1958. AN EXPERIMENTAL INVESTIGATION OF FACTORS AFFECTING ELASTIC WAVE VELOCITIES IN POROUS MEDIA, *Geophysics*, 23, 459-493.
- Wyllie, M., Gregory, A. & Gardner, L., 1956. ELASTIC WAVE VELOCITIES IN HETEROGENEOUS AND POROUS MEDIA, *Geophysics*, 21, 41-70.
- Zheng, P., Ding, B. & Sun, X., 2017. Elastic wave attenuation and dispersion induced by mesoscopic flow in double-porosity rocks, *Int J Rock Mech Min*, 91, 104-111.

Appendix A. Constitutive relationship of double porosity porous medium

Assuming the porous medium is isotropic and pore fluids have no shear strains, the relationship among changes in total stress $d\boldsymbol{\sigma}$, solid stress $d\boldsymbol{\sigma}_s$ and fluid pressure dp in are governed by (Terzaghi, 1943, Biot, 1941):

$$\begin{aligned} d\boldsymbol{\sigma}_1 &= d\boldsymbol{\sigma}_{s1} - \alpha dp_1 \\ d\boldsymbol{\sigma}_2 &= d\boldsymbol{\sigma}_{s2} - \alpha dp_2 \end{aligned} \quad \text{A (1)}$$

Here subscripts 1 and 2 refer to phases with different porosity. In the case of linear elasticity, the stress-strain relationships of solid phases are defined as:

$$\begin{aligned} d\boldsymbol{\sigma}_{s1} &= \mathbf{M}_1 d\mathbf{e}_1, \\ d\boldsymbol{\sigma}_{s2} &= \mathbf{M}_2 d\mathbf{e}_2, \end{aligned} \quad \text{A (2)}$$

where e_x is solid strain. The total strain in double porosity matrix due to strains in each of the phases is:

$$\int_{\Omega_1 + \Omega_2} d\mathbf{e} dv = \int_{\Omega_1} d\mathbf{e}_1 dv + \int_{\Omega_2} d\mathbf{e}_2 dv = \int_{\Omega_1} \mathbf{M}_1^{-1} (d\boldsymbol{\sigma}_1 + \alpha dp_1) dv + \int_{\Omega_2} \mathbf{M}_2^{-1} (d\boldsymbol{\sigma}_2 + \alpha dp_2) dv, \quad \text{A (3)}$$

where Ω_m is the space of phase m . Considering the equilibrium condition of local stress, the stress changes in nearby phases satisfy $d\boldsymbol{\sigma}_1 = d\boldsymbol{\sigma}_2 = d\bar{\boldsymbol{\sigma}}$. If the local strain in phase m is homogeneous, the integral are to be replaced by volume fraction v_1, v_2 . The total strain is

$$\mathbf{e} = v_1 \mathbf{e}_1 + v_2 \mathbf{e}_2 = (v_1 \mathbf{M}_1^{-1} + v_2 \mathbf{M}_2^{-1}) \bar{\boldsymbol{\sigma}} + v_1 \alpha \mathbf{M}_1^{-1} p_1 + v_2 \alpha \mathbf{M}_2^{-1} p_2, \quad \text{A (4)}$$

or

$$\bar{\boldsymbol{\sigma}} = (v_1 \mathbf{M}_1^{-1} + v_2 \mathbf{M}_2^{-1})^{-1} (\mathbf{e} - v_1 \alpha \mathbf{M}_1^{-1} p_1 - v_2 \alpha \mathbf{M}_2^{-1} p_2). \quad \text{A (5)}$$

For uniaxial deformation in the x -direction ($e_y = e_z = 0$), we have

$$\bar{\sigma}_x = \bar{M} \frac{du}{dx} - \alpha'_1 p_1 - \alpha'_2 p_2, \quad \text{A (6)}$$

where $\bar{M} = \frac{M_1 M_2}{v_1 M_2 + v_2 M_1}$, $\alpha'_1 = \frac{v_1 \bar{M}}{M_1} \alpha$, $\alpha'_2 = \frac{v_2 \bar{M}}{M_2} \alpha$, $M_m = 2G_m \frac{1 - \nu_m}{1 - 2\nu_m}$, $m=1,2$.

The relationship among pore fluid pressure p , solid strain \mathbf{e} and fluid content variation ξ are governed by (Biot, 1956, Sun *et al.*, 2016)

$$s_1 = R_1 \xi + \sigma'_1, \quad ,$$

$$s_2 = R_2 \xi_2 + \sigma'_2 \quad , \quad \text{A (7)}$$

where the stress on fluid is $s_m = \phi_m p_m$ and $\sigma'_m = Q_m I_1, m=1,2$. $I_1 = e_x + e_y + e_z, R_m, Q_m$ are elastic constant as proposed in Biot's work(Biot, 1956). The σ'_m is a measure of the change in pore fluid pressure for solid strain. In long-time equilibrium condition, the change of fluid pressure changes relax to a stable value σ' . Without the lose of generality, we have $\sigma'_1 = \sigma' = \sigma'_2 / \beta^*$ and $\beta^* = Q_2 / Q_1$.

The total fluid content variation due to that in each of the phase is

$$\xi = v_1 \xi_1 + v_2 \xi_2 = - \left(\frac{v_1}{R_1} + \frac{v_2}{R_2} \beta \right) \sigma' + \frac{v_1}{R_1} s_1 + \frac{v_2}{R_2} s_2, \quad \text{A (8)}$$

or

$$R' \xi + \sigma' = \frac{R'}{R_1} v_1 s_1 + \frac{R'}{R_2} v_2 s_2, \quad \text{A (9)}$$

where $R' = \frac{R_1 R_2}{v_1 R_2 + v_2 R_1 \beta^*}$. The stress on fluid caused by fluid content variation in each phase

is defined as $s' = R' \xi + \sigma'$. The total stress of porous medium are separated into solid part σ_x and fluid part s' .

$$\bar{\sigma}_x = \sigma_x - s' = \sigma_x - \frac{R'}{R_1} v_1 \sum_{m=1}^2 \phi_m p_1 - \frac{R'}{R_2} v_2 \sum_{m=1}^2 \phi_m p_2. \quad \text{A (10)}$$

Combining A (6) and A (10), we have

$$\sigma_x = \bar{M} \frac{du}{dx} - \gamma_1 p_1 - \gamma_2 p_2 \quad , \quad \text{A (11)}$$

where $\gamma_1 = \frac{\bar{M}}{M_1} v_1 \alpha - \frac{R'}{R_1} v_1 \sum_{m=1}^2 \phi_m$, $\gamma_2 = \frac{\bar{M}}{M_2} v_2 \alpha - \frac{R'}{R_2} v_2 \sum_{m=1}^2 \phi_m$, $\bar{M} = \frac{M_1 M_2}{v_1 M_2 + v_2 M_1}$.

Since we have

$$\frac{\bar{M} v_1}{M_1} = \frac{v_1 M_2}{v_1 M_2 + v_2 M_1} = \frac{v_1 \phi_{10}}{v_1 \phi_{10} + v_2 \phi_{20}} \frac{\phi_{10} M_1}{\phi_{20} M_2} = \frac{\phi_1}{\phi_1 + \phi_2} \frac{\phi_{10} M_1}{\phi_{20} M_2},$$

$$\frac{R' v_1}{R_1} = \frac{v_1 R_2}{v_1 R_2 + v_2 R_1 \beta^*} = \frac{\phi_1}{\phi_1 + \phi_2} \frac{\phi_{10} R_1 \beta^*}{\phi_{20} R_2},$$

We define

$$\beta = \frac{M_1 \phi_{10}}{M_2 \phi_{20}} = \frac{R_1 \phi_{10}}{R_2 \phi_{20}} \beta^* . \quad \text{A (12)}$$

The coefficients γ_1, γ_2 can be rewritten as

$$\gamma_1 = \left(\alpha - \sum_{m=1}^2 \phi_m \right) \frac{\phi_1}{\phi_1 + \phi_2 \beta} , \quad \text{A (13)}$$

$$\gamma_2 = \left(\alpha - \sum_{m=1}^2 \phi_m \right) \frac{\phi_2}{\phi_2 + \phi_1 / \beta} . \quad \text{A (14)}$$

The parameter α is defined as $\alpha = \frac{2(1+\nu)G}{3(1-2\nu)Q} = \frac{K}{Q}$ (Biot, 1941, Dvorkin and Nur, 1993),

where $\frac{1}{Q} = \frac{1}{K} - \frac{1}{K_s}$. Here ν_1, ν_2 are the volume fraction of the phase 1 (inner pocket) and phase 2 (surrounding patch) respectively. Here ν is Poisson's ratio, G is shear modulus and K is bulk modulus. Q is elastic constants. $\bar{\sigma}_x, \bar{\sigma}_y, \bar{\sigma}_z$ are total stress in the porous medium. p is the fluid pressures inside the immiscible fluid patches.

The conservation equations in partially saturated double-porosity medium are given as

$$\begin{aligned} \frac{\partial(\rho_{f_1} \phi_1)}{\partial t} + \frac{\partial[\rho_{f_1}(q_x^{(1)} - \phi_1 \dot{u}_x)]}{\partial x} + \frac{\partial(\rho_{f_1} q_r^{(1)})}{\partial r} + \frac{\rho_{f_1} q_r^{(1)}}{r} &= 0 \\ \frac{\partial(\rho_{f_2} \phi_2)}{\partial t} + \frac{\partial[\rho_{f_2}(q_x^{(2)} - \phi_2 \dot{u}_x)]}{\partial x} + \frac{\partial(\rho_{f_2} q_r^{(2)})}{\partial r} + \frac{\rho_{f_2} q_r^{(2)}}{r} &= 0 \end{aligned} , \quad \text{A (15)}$$

where $q_x^{(1)} = \phi_1(\dot{U}_x^{(1)} - \phi_2 \dot{Z}_x)$ and $q_x^{(2)} = \phi_2(\dot{U}_x^{(2)} + \phi_1 \dot{Z}_x)$ are the volumetric flux rate in the x-directions within the fluid patches. Here $q_r^{(1)} = \phi_1 \dot{U}_r^{(1)}$ and $q_r^{(2)} = \phi_2 \dot{U}_r^{(2)}$ are in the r-directions. A linearization gives

$$\begin{aligned} \frac{\phi_1}{\rho_{f_1}} \frac{\partial \rho_{f_1}}{\partial t} + \frac{\partial \phi_1}{\partial t} + \phi_1 \frac{\partial^2 (U_x^{(1)} - \phi_2 Z_x - u_x)}{\partial t \partial x} + \phi_1 \left(\frac{\partial^2 (U_r^{(1)})}{\partial t \partial r} + \frac{1}{r} \frac{\partial (U_r^{(1)})}{\partial t} \right) &= 0 \\ \frac{\phi_2}{\rho_{f_2}} \frac{\partial \rho_{f_2}}{\partial t} + \frac{\partial \phi_2}{\partial t} + \phi_2 \frac{\partial^2 (U_x^{(2)} + \phi_1 Z_x - u_x)}{\partial t \partial x} + \phi_2 \left(\frac{\partial^2 (U_r^{(2)})}{\partial t \partial r} + \frac{1}{r} \frac{\partial (U_r^{(2)})}{\partial t} \right) &= 0 \end{aligned} , \quad \text{A (16)}$$

The variation in fluid content, i.e., the porosity change is $d\phi_m = \alpha \frac{\partial u}{\partial x} + \frac{p_m}{H'_m}$, (m=1,2). Here

$$H'_1 = H_1 + H_1 \phi_2 \beta / \phi_1 , \quad H'_2 = H_2 + H_2 \phi_1 / (\beta \phi_2) , \quad 1/H_m = \left(1 - \sum_{m=1}^2 \phi_m - K/K_s \right) / K_s .$$

The porosity differential is

$$\frac{d\phi_m}{dt} = \alpha \frac{\partial^2 u_x}{\partial x \partial t} + \frac{1}{H'_m} \frac{\partial p_m}{\partial t}. \quad \text{A (17)}$$

The fluid density compressibility is represented as $d\rho_f = \frac{dp}{c_0^2}$, where c_0 is acoustic velocity of fluid.

By substituting $\frac{d\phi}{dt}$ and $d\rho_f$ into Eq. (7), we have

$$\begin{aligned} \frac{dp_1}{dt} &= -F_1 \left(\frac{\partial^2 (U_x^{(1)} - \phi_2 Z_x)}{\partial t \partial x} + \frac{\partial^2 (U_r^{(1)})}{\partial t \partial r} + \frac{1}{r} \frac{\partial (U_r^{(1)})}{\partial t} + \frac{\gamma_1}{\phi_1} \frac{\partial^2 u_x}{\partial t \partial x} \right) \\ \frac{dp_2}{dt} &= -F_2 \left(\frac{\partial^2 (U_x^{(2)} + \phi_1 Z_x)}{\partial t \partial x} + \frac{\partial^2 (U_r^{(2)})}{\partial t \partial r} + \frac{1}{r} \frac{\partial (U_r^{(2)})}{\partial t} + \frac{\gamma_2}{\phi_2} \frac{\partial^2 u_x}{\partial t \partial x} \right), \end{aligned} \quad \text{A (18)}$$

$$\text{where } F_1 = \frac{K_{f_1} (\phi_1 + \phi_2 \beta) H_1}{K_{f_1} + (\phi_1 + \phi_2 \beta) H_1}, F_2 = \frac{K_{f_2} (\phi_2 + \phi_1 / \beta) H_2}{K_{f_2} + (\phi_2 + \phi_1 / \beta) H_2}.$$

We have eight unknowns $U_x^{(1)}, U_x^{(2)}, U_r^{(1)}, U_r^{(2)}, u_x, Z_x, p_1, p_2$ and eight differential equations.

In the case of plane-wave propagation, the displacements and pressure are expressed by wave kernel $e^{i(\alpha t - \mathbf{k} \cdot \mathbf{x})}$

$$\begin{aligned} u_x(x, t) &= C_1 e^{i(\alpha t - \mathbf{k} \cdot \mathbf{x})}, & U_x^{(1)}(x, t) &= C_2^{(1)} e^{i(\alpha t - \mathbf{k} \cdot \mathbf{x})} \\ U_x^{(2)}(x, t) &= C_2^{(2)} e^{i(\alpha t - \mathbf{k} \cdot \mathbf{x})}, & Z_x(x, t) &= C_3 e^{i(\alpha t - \mathbf{k} \cdot \mathbf{x})} \\ U_r^{(1)}(x, r, t) &= U_{r0}^{(1)}(r) e^{i(\alpha t - \mathbf{k} \cdot \mathbf{x})}, & U_r^{(2)}(x, r, t) &= U_{r0}^{(2)}(r) e^{i(\alpha t - \mathbf{k} \cdot \mathbf{x})} \\ p_1(x, r, t) &= p_{01}(r) e^{i(\alpha t - \mathbf{k} \cdot \mathbf{x})}, & p_2(x, r, t) &= p_{02}(r) e^{i(\alpha t - \mathbf{k} \cdot \mathbf{x})} \end{aligned} \quad \text{A (19)}$$

Then we have

$$\begin{aligned} \frac{\partial p_{01}}{\partial r} &= U_{r0}^{(1)} \rho_{f_1} \omega^2 \left(\frac{1 + 1/\phi_{10}}{2} - i \frac{\omega_c^{(1)}}{\omega} \right) \\ \frac{\partial p_{02}}{\partial r} &= U_{r0}^{(2)} \rho_{f_2} \omega^2 \left(\frac{1 + 1/\phi_{20}}{2} - i \frac{\omega_c^{(2)}}{\omega} \right), \end{aligned} \quad \text{A (20)}$$

$$\text{where } \omega_c^{(m)} = \frac{\mu_m \phi_{m0}}{\rho_{fm} K_m}, \quad m=1,2.$$

And the ordinary differential equations of p_{01} and p_{02} are

$$\begin{aligned} \frac{\partial^2 p_{01}}{\partial r^2} + \frac{1}{r} \frac{\partial p_{01}}{\partial r} + \frac{\rho_{f_1} \omega^2}{F_1} \left(\frac{1 + 1/\phi_{10}}{2} - i \frac{\omega_c^{(1)}}{\omega} \right) p_{01} - ik \rho_{f_1} \omega^2 \left(C_2^{(1)} - \phi_2 C_3 + \frac{\gamma_1}{\phi_1} C_1 \right) \left(\frac{1 + 1/\phi_{10}}{2} - i \frac{\omega_c^{(1)}}{\omega} \right) &= 0 \\ \frac{\partial^2 p_{02}}{\partial r^2} + \frac{1}{r} \frac{\partial p_{02}}{\partial r} + \frac{\rho_{f_2} \omega^2}{F_2} \left(\frac{1 + 1/\phi_{20}}{2} - i \frac{\omega_c^{(2)}}{\omega} \right) p_{02} - ik \rho_{f_2} \omega^2 \left(C_2^{(2)} + \phi_1 C_3 + \frac{\gamma_2}{\phi_2} C_1 \right) \left(\frac{1 + 1/\phi_{20}}{2} - i \frac{\omega_c^{(2)}}{\omega} \right) &= 0 \end{aligned} \quad \text{A (21)}$$

Appendix B. Plane wave analysis equations

The coefficients are:

$$\begin{aligned}
 S_1 &= \frac{\phi_2 \phi_2 \phi_1 (\chi_1 \omega^2 - i\beta_1 \omega)}{3} + \phi_1 \phi_2 (\tilde{F}_1 \phi_2 + \tilde{F}_2 \phi_1) , \\
 S_{10} &= \frac{\phi_2 \phi_{20} \phi_{10} (\chi_1 \omega^2 - i\beta_1 \omega)}{3} + \phi_{10} \phi_{20} (\tilde{F}_1 \phi_2 + \tilde{F}_2 \phi_1) , \\
 S_2 &= \tilde{F}_2 \gamma_{20} \phi_1 \nu_2 - \tilde{F}_1 \gamma_{10} \phi_2 \nu_1 , \quad S_{20} = \tilde{F}_2 \gamma_{20} \phi_{10} - \tilde{F}_1 \gamma_{10} \phi_{20} , \\
 a_{11} &= \bar{M} - \frac{S_2 S_{20}}{S_{10}} + \frac{\tilde{F}_1 \gamma_1 \gamma_{10}}{\phi_{10}} + \frac{\tilde{F}_2 \gamma_2 \gamma_{20}}{\phi_{20}} , \quad a_{12} = a_{21} = \tilde{F}_1 \gamma_1 + \frac{\tilde{F}_1 \phi_{10} \phi_{20} S_2}{S_{10}} , \\
 a_{13} &= a_{31} = \tilde{F}_2 \gamma_2 + \frac{\tilde{F}_2 \phi_{10} \phi_{20} S_2}{S_{10}} , \quad a_{22} = \tilde{F}_1 \phi_1 \left(1 - \frac{\tilde{F}_1 \phi_{10} \phi_{20} \phi_2}{S_{10}} \right) , \\
 a_{23} &= a_{32} = \frac{\tilde{F}_1 \tilde{F}_2 \phi_{10} \phi_{20} \phi_1 \phi_2}{S_{10}} , \quad a_{33} = \tilde{F}_2 \phi_2 \left(1 - \frac{\tilde{F}_2 \phi_{10} \phi_{20} \phi_1}{S_{10}} \right) , \quad \text{B (1)}
 \end{aligned}$$

where $\tilde{F}_m = F_m \left(1 - \frac{2J_1(\lambda_m R)}{\lambda_m R J_0(\lambda_m R)} \right)$, $F_1 = \frac{K_{f_1} (\phi_1 + \phi_2 \beta) H_1}{K_{f_1} + (\phi_1 + \phi_2 \beta) H_1}$, $F_2 = \frac{K_{f_2} (\phi_2 + \phi_1 / \beta) H_2}{K_{f_2} + (\phi_2 + \phi_1 / \beta) H_2}$. We

use $\phi_1 = \phi_{10} \nu_1$, $\phi_2 = \phi_{20} \nu_2$, $\gamma_1 = \gamma_{10} \nu_1$, $\gamma_2 = \gamma_{20} \nu_2$, $\gamma_{10} = \left(\alpha - \sum_{m=1}^2 \phi_m \right) \frac{\phi_{10}}{\phi_1 + \phi_2 \beta}$ and

$\gamma_{20} = \left(\alpha - \sum_{m=1}^2 \phi_m \right) \frac{\phi_{20}}{\phi_2 + \phi_1 / \beta}$ in deriving the coefficients.

The coefficients A, B, C, D are

$$A = a_{11} a_{22} a_{33} - a_{11} a_{23} a_{32} - a_{12} a_{21} a_{33} + a_{12} a_{23} a_{31} + a_{13} a_{21} a_{32} - a_{13} a_{22} a_{31} \quad \text{B (2)}$$

$$\begin{aligned}
 B &= a_{11} a_{22} b_{33} - a_{11} a_{23} b_{32} - a_{11} a_{32} b_{23} + a_{11} a_{33} b_{22} - a_{12} a_{21} b_{33} + a_{12} a_{23} b_{31} \\
 &+ a_{12} a_{31} b_{23} - a_{12} a_{33} b_{21} + a_{13} a_{21} b_{32} - a_{13} a_{22} b_{31} - a_{13} a_{31} b_{22} + a_{13} a_{32} b_{21} \\
 &+ a_{21} a_{32} b_{13} - a_{21} a_{33} b_{12} - a_{22} a_{31} b_{13} + a_{22} a_{33} b_{11} + a_{23} a_{31} b_{12} - a_{23} a_{32} b_{11}
 \end{aligned} \quad \text{B (3)}$$

$$\begin{aligned}
 C &= a_{11} b_{22} b_{33} - a_{11} b_{23} b_{32} - a_{12} b_{21} b_{33} + a_{12} b_{23} b_{31} + a_{13} b_{21} b_{32} - a_{13} b_{22} b_{31} \\
 &- a_{21} b_{12} b_{33} + a_{21} b_{13} b_{32} + a_{22} b_{11} b_{33} - a_{22} b_{13} b_{31} - a_{23} b_{11} b_{32} + a_{23} b_{12} b_{31} \\
 &+ a_{31} b_{12} b_{23} - a_{31} b_{13} b_{22} - a_{32} b_{11} b_{23} + a_{32} b_{13} b_{21} + a_{33} b_{11} b_{22} - a_{33} b_{12} b_{21}
 \end{aligned} \quad \text{B (4)}$$

$$D = b_{11} b_{22} b_{33} - b_{11} b_{23} b_{32} - b_{12} b_{21} b_{33} + b_{12} b_{23} b_{31} + b_{13} b_{21} b_{32} - b_{13} b_{22} b_{31} \quad \text{B (5)}$$